# Wideband Radiometry From P to S Band for Monitoring Polar Regions

By Giovanni Macelloni, *Senior Member IEEE*, Kenneth C. Jezek, Marco Brogioni, *Member IEEE*, Joel T. Johnson, *Fellow IEEE*, Marion Leduc-Leballeur, Ghislain Picard, Ange Haddjeri, Lars Kaleschke, Jacqueline Boutin, *Member IEEE*, Jean Luc Vergely, Nicolas Kolodziejczyk, Laurent Bertino, Emmanuel P. Dinnat, *Senior Member IEEE*, Rasmus T. Tonboe, Anne Munck Solgaard, Xiaoji Shen, *Member IEEE*, Jeffrey P. Walker, *Fellow IEEE*, Synne Høyer Svendsen, Stef Lhermitte, and Yiwen Zhou, *Senior Member IEEE*

**ABSTRACT** | This article reviews existing and planned contributions of spaceborne microwave radiometry from P to S band to new measurements of key geophysical variables with a particular focus on the polar regions. It summarizes the current state of spaceborne microwave radiometry to measure ice sheet thermal states, sea ice thickness (SIT), salinity, and sea surface salinity (SSS). Then, this article discusses the potential of wideband radiometry, with continuous sampling in the range of 0.4–2 GHz, as a breakthrough for enhancing the estimation of geophysical variables such as SSS and the geothermal heat flux beneath the polar ice sheets, which are currently monitored primarily using L-band radiometry satellites. Furthermore, this article describes opportunities for new unique observations that cannot be achieved with the current constellation of satellite sensors. In addition, this article demonstrates the advantages of using low-frequency radiometry in sensing soil moisture and biomass from space due to the great sensing depth. This article concludes with a discussion of mission concepts highlighting the CryoRad mission, which has been selected as one of the four candidates for European Space Agency Earth Explorer 12 competition and is now conducting Phase 0 feasibility studies, envisions a 0.4–2-GHz dedicated spaceborne radiometer operated with circular polarization.

**KEYWORDS** | Cryosphere; microwave radiometry; new missions; sea surface salinity (SSS); wideband.

## I. INTRODUCTION

Polar regions are critical parts of the rapidly changing Earth system. Mass loss from the Greenland and Antarctic ice sheets now constitutes a major contribution to sea-level rise [1]. The instability of ice shelves—the outer floating part of the ice sheets—and their potential future collapse poses additional risks for accelerating ice sheet discharge and sea-level rise even further [2]. In parallel, the reduction of sea ice extent and thickness in both the Arctic [3] and the Antarctic [4], along with declining snow cover and rising permafrost temperatures, are strong indicators of the continuing degradation of the cryosphere [5]. Some of these changes are associated with the warming of oceans, while the Southern Ocean plays a dominant role in the total heat gain by the global ocean [6], [7].

Received 1 July 2025; revised 21 November 2025 and 2 January 2026; accepted 2 January 2026. This work was supported in part by the CryoRad Earth Explorer 12 Phase 0 Science and Requirements Consolidation Study (SciReC) through European Space Agency (ESA) under Grant 4000145903/24/NL/IB/ar and in part by the National Aeronautics and Space Administration (NASA) through WBS under Grant 970834.05.01.01.02. The work of Kenneth C. Jezek and Joel T. Johnson was supported in part by NASA's Instrument Incubator under Grant NNX14AE68G and in part by Cryospheric Science Programs under Grant 80NSSC18K0550 and Grant NNX14AH91G. The ISSIUMAX Project was supported by Italian Antarctic Program [Programma Nazionale di Ricercerche in Antartide (PNRA)] under Contract 2016/AZ3.02. The work of Jacqueline Boutin and Jean Luc Vergely was supported by the Centre National D'Etudes Spatiales (CNES) Research and Technology Funding through Etude de la salinité en mers froides par radiométrie multibande 0.4–2 GHz. *(All the authors contributed equally to this work.) (Corresponding author: Giovanni Macelloni.)*
Please see the Acknowledgment section of this article for the author affiliations.

Digital Object Identifier 10.1109/JPROC.2026.3653571

The combined effects of land ice melting and sea ice decline have altered ocean–atmosphere interactions. These changes enhance ocean heat storage, intensify the freshwater cycle, and modify ocean stratification. In turn, this cascade of processes affects sea-ice dynamics and ocean overturning circulation, with implications for both regional and global climate systems. Dense, saline waters formed in polar regions feed the abyssal layer of the global ocean, transport heat between hemispheres, and help regulate atmospheric carbon dioxide concentrations [2], [8]. Through their impacts on sea level and ocean convection, the consequences of these changes in polar regions are global, impacting weather patterns, climate, and ecosystems worldwide.

The global significance of polar regions is further underscored by McKay et al. [9], which identified polar regions as containing many of Earth's climate tipping points, critical thresholds beyond which a change would significantly alter the Earth system and impact human welfare. A deeper understanding of how and when such tipping points might be reached, as well as the potential impacts of mitigation and adaptation strategies, requires improved observational capabilities and process-level knowledge of the cryosphere. Despite considerable advances over the last decade, especially in weather and climate modeling, substantial uncertainties persist in our understanding of cryospheric processes. These uncertainties largely stem from a lack of high-quality observations of key physical parameters at the temporal and spatial scales necessary for the next-generation assimilation and predictive monitoring. Due to the cryosphere's vast extent, remoteness, and extreme environmental conditions, satellite observations have long been crucial for understanding cryospheric processes. The abilities of spaceborne microwave sensors to provide all-weather, day-and-night observations have made them especially valuable. Recent achievements include the use of interferometric synthetic aperture radar (InSAR) to map ice sheets, delineate grounding lines, and monitor sea ice motion, as well as the use of radar altimetry to measure the thickness of both sea ice and polar ice sheets [10].

Spaceborne microwave radiometers have also been extensively employed due to their extensive spatial coverage and short revisit time, enabling weekly or subweekly observations. Before 2009, the lowest available frequency for passive microwave observations from space was 6.8 GHz (∼5-cm wavelength), limiting emission to being from the upper tens of meters in ice sheets/shelves, centimeters in sea ice, and very low sensitivity to ocean salinity. The introduction of L-band (1.4 GHz) spaceborne radiometers on missions such as ESA's Soil Moisture and Ocean Salinity (SMOS) (2009), NASA/CONAE's Aquarius (2011), and NASA's Soil Moisture Active Passive (SMAP) (2015) significantly expanded remote sensing capabilities over polar regions. These instruments, originally designed for SMOS monitoring, also provided information from deeper layers in ice, snow, and frozen soil compared to sensors operating at higher frequencies (e.g., SMMR, SSM/I, AMSR-E, AMSR2, and the future MWI aboard MetOp-SG). This enhanced sensing capability has enabled several key cryospheric studies, such as inferring subsurface ice sheet temperature [11], [12], detecting sea ice thickness (SIT) in the critical 0–1-m range where the uncertainty of satellite altimetry is high [13] identifying freeze/thaw cycles of permafrost [14], [15], and detecting subsurface meltwater and aquifers in ice sheets and shelves [16].

Although this progress has yielded significant and new geophysical results and applications, important limitations remain. The emission depth for L-band signals is not sufficient for thick ice sheets [11]. For example, ice sheet temperature estimation at L band becomes inaccurate below 1000–1500 m depth, which is insufficient for characterizing the full thickness of many parts of the Antarctic and Greenland ice sheets. At depths beyond 2500 m, temperature uncertainty can exceed 8 K in some locations although it remains below 2 K in approximately 75% of cases [12]. For sea ice, a data fusion approach, which combines SMOS and CryoSat observations, can potentially yield ice thickness estimates with less than 30% uncertainty for very thin ($<$50 cm) or thick ($>$1 m) ice [17]. However, the accuracy drops for intermediate thicknesses (50–100 cm), falling short of the Global Climate Observing System (GCOS) threshold and goal uncertainty requirements, which are 25 and 10 cm, respectively [18]. For sea surface salinity (SSS), the uncertainty increases in polar regions because the sensitivity of the measured brightness temperature (TB, primarily a function of surface emissivity and physical temperature) sensitivity to SSS decreases by about a factor of three from warm to cold water [19], [20], [21], [22]. To overcome these limitations, new ideas have emerged to extend observations to lower microwave frequencies and expand the observational bandwidth [23]. This approach enables greater emission depths for glaciers and sea ice and improves sensitivity to SSS in cold water. In particular, a wideband radiometer operating between 0.4 and 2 GHz offers two major advantages. First, although this frequency range is more susceptible to radio frequency interference (RFI) [24], continuous sampling across narrow subbands allows for the extraction of uncontaminated TB data. Second, wideband data enable new retrieval approaches based on spectral properties of the surface and subsurface, similar to hyperspectral methods in the optical domain, or atmospheric sounding in the thermal and microwave domains. The rich spectral information enables simultaneous retrieval of multiple variables, such as the ice temperatures at different depths within the ice sheet, while reducing the risk of ill-conditioning. At microwave frequencies, the achievable spatial resolution is fundamentally constrained by the diffraction limit, which scales with wavelength and antenna aperture size. Previously, using these lower frequencies from space was considered impractical due to the inherently coarse resolution dictated by the diffraction limit and by technological constraints on antenna size. However, synthetic aperture techniques, such as those employed by ESA's SMOS mission, have demonstrated the feasibility of achieving higher spatial

resolution at L band. Moreover, recent advances in large deployable antenna systems, implemented on missions such as NASA's SMAP (L band) and ESA's copernicus imaging microwave radiometer (CIMR) and Biomass, further extend the potential for high-resolution observations at L band and below, making spaceborne radiometry at these frequencies increasingly practical.

This article summarizes recent progress in wideband, low-frequency radiometry; provides scientific rationale for its application to cryospheric and related Earth system processes; and describes the technical implementation of future spaceborne missions based on this emerging observational approach.

## II. CAPABILITIES OF LOW-FREQUENCY MICROWAVE RADIOMETERS

Microwave thermal emission at low frequencies exhibits increased emission depth into geophysical media, as detailed in [23]. Specifically, frequencies below the 1.4-GHz protected band—used in missions such as SMOS, Aquarius, and SMAP—allow for significantly greater emission depths in soil, sea ice, and ice sheets. For example, in wet soil, the emission depth at 0.4 GHz is approximately 50% greater than at 1.4 GHz. In compacted sea ice (up to 1 m thick), the increase is around 100%, while in ice sheets, it exceeds 300% [23]. This greater depth of emission improves the sensitivity of radiometric measurements to subsurface properties, enabling more accurate retrievals of variables such as soil moisture, SIT, and internal ice sheet temperature profiles. For SSS, lower frequencies also offer improved sensitivity in cold water environments. At 0.4 GHz, the sensitivity to salinity is approximately three times higher than at 1.4 GHz in high-salinity conditions, and even greater in low-salinity waters. In Sections II-A–II-D, the observational capabilities and scientific motivations for adopting wide-band, low-frequency microwave radiometry are reviewed. The focus is on cryospheric and polar ocean parameters corresponding to the main objectives of current mission proposals; however, information on soil and vegetation parameters are also provided.

### A. Ice Sheet and Shelves

*1) Background:* Satellite observations over the past three decades have documented an accelerating loss of mass from both the Greenland and Antarctic ice sheets. Studies that couple ice sheet modeling with climate modeling indicate that this acceleration is likely to continue well beyond the end of the century, particularly under high greenhouse gas emissions scenarios [25]. Even under pathways consistent with Paris Climate Agreement targets, projections suggest that mass loss from these ice sheets will remain one of the dominant contributors to future global mean sea-level rise [2]. Uncertainties in the sea-level rise contribution from land ice have been quantitatively assessed in [25], who evaluated a range of climate scenarios and ice sheet/glacier model combinations for estimating sea level by 2100. While projections for mountain glaciers remain relatively consistent across scenarios, estimates for the Greenland and Antarctic ice sheets vary widely, with projected sea-level contributions ranging from 12 to 42 cm by 2100 under risk-averse assumptions. This uncertainty reflects a limited understanding of key rate-controlling processes.

Antarctica's contribution is even more uncertain and spans a broader range of outcomes, due to the complex and poorly understood processes governing ice–ocean interactions and ice sheet dynamics. The study given in [25] emphasizes that variability in basal melting beneath ice shelves is the dominant source of uncertainty in Antarctic projections. These basal processes govern the thinning and collapse of ice shelves, which, in turn, regulate the discharge from grounded ice upstream. Additional uncertainty stems from the parameterization of ice sheet dynamics. Consequently, improved observations and model constraints are urgently needed to better characterize Antarctic basal processes, ice shelf stability, and their coupling with the ocean. International research programs have proposed strategies to reduce these uncertainties, and significant progress has been reported [26]. However, major uncertainties remain related to a limited quantitative understanding of many of the processes that control the mass balance and stability of ice sheets, and the inability to characterize such processes from space using existing or planned sensors [25], [27], [28].

Within the Ice Sheet Model Intercomparison Project (ISMIP6 ensemble of future projections [28]), the dominant sources of uncertainty for ice sheets include surface forcing, ice–ocean interaction, model initialization, and representation of subgrid physics [25], [27], [28]. Many of these uncertainties are associated with poorly understood processes, such as basal hydrology and sliding, ice–water interactions, and meltwater routing. A persistent limitation is the lack of observations for two key physical parameters: englacial temperature, which directly influences ice viscosity and deformation rates, and basal thermal state, which controls whether the ice is frozen to the bed or capable of sliding.

Englacial and basal ice sheet temperatures are governed by a combination of long-term surface temperature history, upward geothermal flux at the base, vertical and horizontal ice advection, and internal heating processes such as shearing, sliding, and refreezing of meltwater [29], [30]. Yet, direct measurements of these temperatures exist only at a small number of deep boreholes in Greenland and Antarctica [31], [32]. This sparse observational coverage leads to poorly constrained ice thermodynamics, which, in turn, contributes to uncertainty in ice sheet modeling. For example, the basal thermal state—whether the base is frozen or thawed—remains undetermined across large areas [33], limiting the ability to model basal mass balance and predict dynamic responses to climate forcing [34].

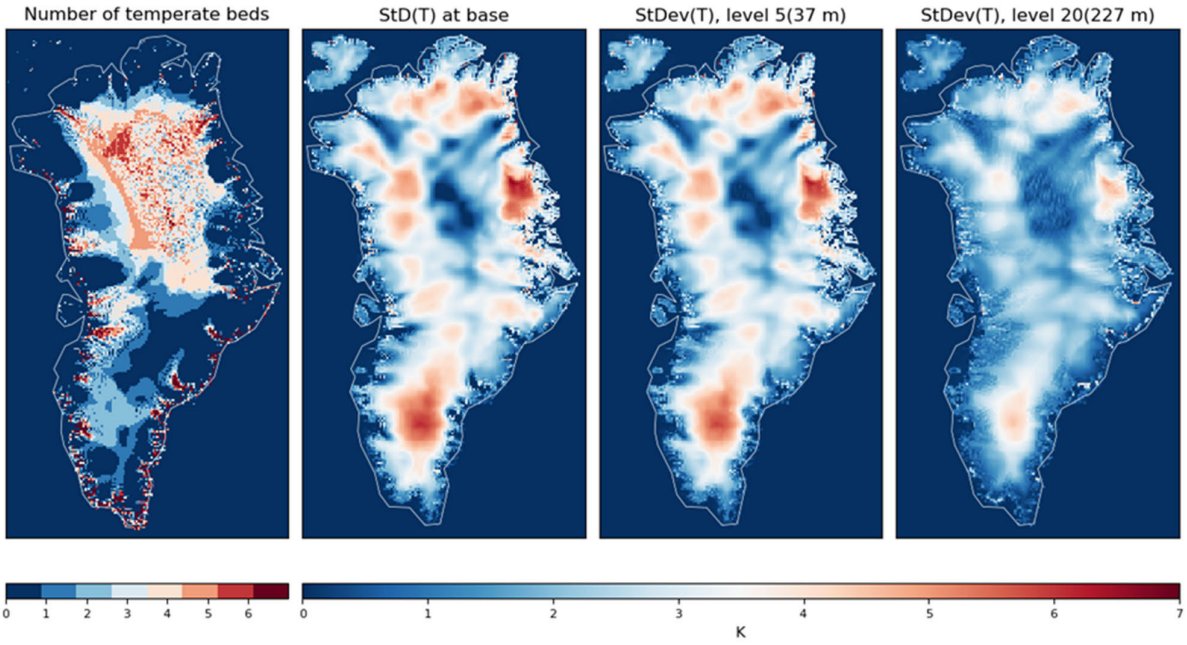


**Fig. 1.** ***Basal thermal state of the Greenland ice sheet (left) and the std of ice temperature at different elevations above the bed from seven glacial cycle spin-up simulations with different geothermal flux maps. Ice flow model: PISM [39], [40] and geothermal flux maps [41], [42], [43], [44], [45], [46].***

Obtaining 3-D observations of the internal temperature field, particularly near the base, would significantly improve the initialization of ice flow models that rely on glacial-cycle spin-up methods and enhance the accuracy of the assimilated basal state when applying inversion techniques. For spin-up approaches, the resulting temperature fields are highly sensitive to assumptions about surface climate history and geothermal heat flux. This sensitivity is demonstrated in Fig. 1, which shows results from seven glacial spin-up simulations using the same ice flow model [parallel ice sheet model (PISM)] and forcing, but with different geothermal heat flux maps. Substantial temperature differences with standard deviation (std) often exceeding 3 K are observed near the bedrock, leading to divergent dynamic behaviors in the modeled ice sheets. Even partial measurements of the 3-D temperature field—limited, for example, to areas with minimal melt or refreezing–would enable the isolation of additional influential variables such as ice fabric, impurity content, geothermal heat flux, and internal damage. These constraints are essential for advancing model fidelity and narrowing the uncertainty in future sea level rise projections.

*2) Microwave Applications:* Significant progress has been made using spaceborne L-band radiometers to infer the glaciological properties of ice sheets and glaciers. For example, SMOS TB data, combined with a thermodynamic model, have been used to infer temperatures within the East Antarctica plateau to a depth of about 1500 m [12]. Additionally, L-band radiometry has been applied in both Greenland and Antarctica to detect meltwater and firn aquifers—perennial liquid water layers trapped within the firn column—which play a crucial role in modulating meltwater transport and contributing to glacier mass balance [35], [36], [37], [38]. Deep water investigation may benefit from lower frequencies due to increased emission depth, but this potential has not been thoroughly tested or explored.

Microwave low-frequency radiometers offer a promising approach to probe temperature deeper, with higher accu-

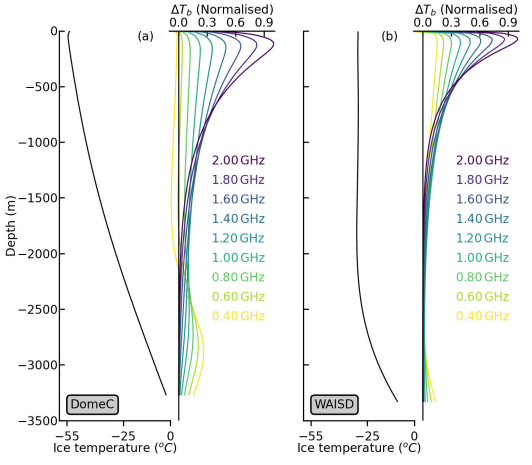


**Fig. 2.** ***Temperature profile and normalized contribution profile (relative to total TB emitted by the ice sheet) for (a) Dome C and (b) WAISD locations.***

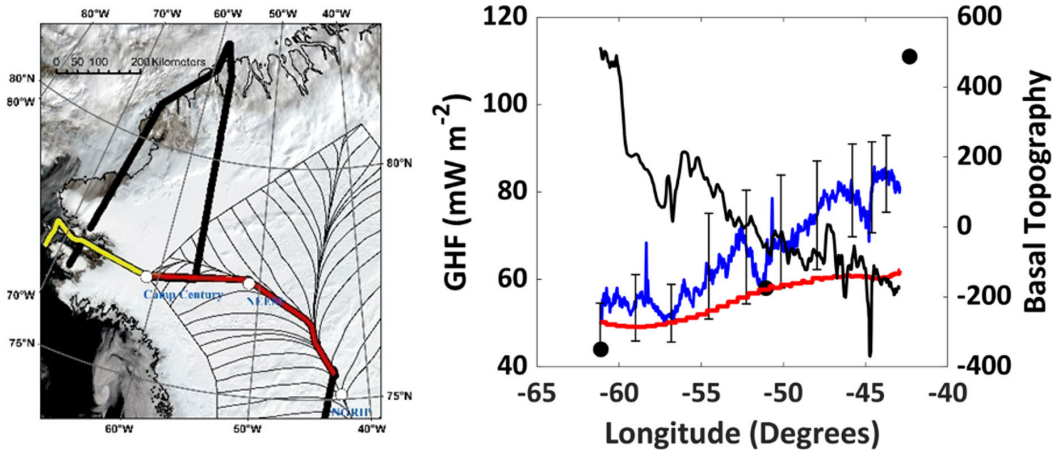


**Fig. 3.** *UWBRAD transects across Greenland (left). The 2016 Greenland flight is shown in yellow. The 2017 Greenland flight is shown in black. The portion of the 2017 line along which intraglacial temperatures were estimated is shown in red. Slope-derived ice-flow lines extending from the ice divides are shown by black thin lines. Retrieved geothermal heat flux (blue) with error bars computed as part of the parameter retrieval (right); black line is the basal topography, while geothermal heat flux from Martos and others (2018) along the transect is in red, and its average at the Camp Century, NEEM, and North GRIP borehole sites are in black circles [52].*

racy. Fig. 2 illustrates the sensitivity of TB as a function of depth into ice, simulated using the snow microwave radiative transfer (RT) model (SMRT [47]) for two distinct sites: 1) Dome C with cold surface conditions and 2) the warmer west antarctic ice sheet (WAIS) divide. Both simulations utilize prescribed temperature profiles from in situ measurements [30] and density profiles derived from in situ data [48] extrapolated at depth using [49]. At the warmer site 2), the contribution is high in the upper part of the ice sheet and generally follows an exponential decay with depth, except very close to the surface. As expected, the contribution at lower frequencies is higher from deeper layers. In contrast, at the colder site [Fig. 2(a)], a distinct secondary peak of sensitivity appears at depth (2500–3200 m) for the lowest frequencies (e.g., 0.4–0.8 GHz). The temperature dependence of complex permittivity, as modeled by Mätzler [50] and used in this SMRT simulation, introduces this increase in absorption with temperature. The cold, overlying ice layers are more transparent and less emissive at such low frequencies, enabling radiation from the underlying warmer and more emissive layers to reach the sensor, resulting in this much deeper contribution to the final signal. These simulations highlight that while higher frequencies probe the near-surface, lower frequencies (e.g., 0.4 GHz) are sensitive to the deep thermal state within the ice column, with the depth sensitivity nonlinearly modulated by the temperature profile in the overlying ice layers. This demonstrates the potential for multifrequency passive microwave observations (combining high and low frequencies) to provide crucial, noninvasive observations on the internal thermal state of ice sheets.

The capability of airborne wideband radiometers to retrieve vertical temperature profiles within ice sheets has been successfully demonstrated in field campaigns over the Greenland ice sheet in 2016 and 2017 using the Ultra-Wideband Software Defined Microwave Radiometer (UWBRAD) [51].

A Bayesian inversion was applied to retrieve geophysical parameters from TB observations [53], using advanced RT models [54], [55] to account for polar firn density layering [54], [55], [56] along with a parameterized ice sheet temperature model [57]. The retrieved results revealed a gradient in basal temperatures along the ice divide from West to East. In this region, the insulating effect of thicker ice layers offsets surface cooling associated with higher elevations. Retrieved basal temperatures increase along the ice divide from West to East, as the insulating effect of thicker ice overcomes surface cooling driven by increasing surface elevation. These retrievals also yielded estimates of basal geothermal heat flux, a key parameter for ice sheet thermodynamics and underlying crustal properties. As shown in Fig. 3, geothermal heat flux values ranged from approximately 50 to 80 mW $\cdot$ m$^{-2}$ along the transect [52]. After applying corrections for internal strain heating, these estimates were reduced by 10–20 mW $\cdot$ m$^{-2}$ and were generally consistent with independent estimates based on magnetic anomaly data.

To date, temperature retrievals using wideband microwave radiometry have been primarily confined to interior ice sheet regions. These areas are characterized by minimal volumetric scattering due to small snow grains compared with the wavelength and relatively homogeneous firn stratigraphy. In such environments, melt and wind crusts are infrequent and can be accounted for using ancillary datasets such as ice cores and ice-penetrating radar [58], [59]. In contrast, near the seaward margins of the ice sheets—where surface melting leads to percolation and refreezing—scattering from embedded ice lenses becomes significant. In regions away from

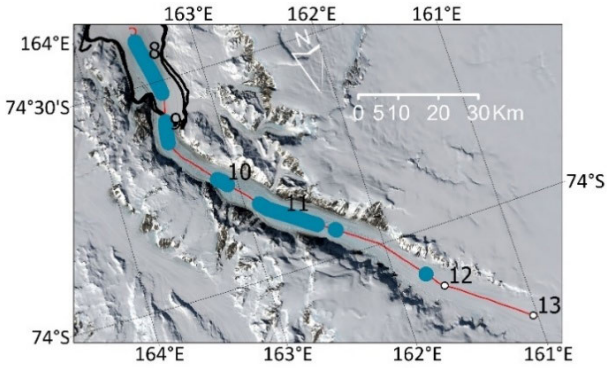


**Fig. 4.** ***Locations of subglacial water inferred from wideband radiometry data along the Priestley Glacier, Northern Victoria Land, Antarctica; adapted from [62].***

crevassed, fast-flowing glaciers, Jezek et al. [60] observed that such scattering reduces TB by up to 40 K relative to the dry snow zone and increases spectral variability, as higher frequencies become increasingly affected. Accurate temperature retrievals in these areas require prior knowledge of scattering properties, which are generally unavailable. However, ice lens characteristics can be estimated using plausible temperature profiles. During the 2016 airborne UWBRAD experiment (yellow line in Fig. 3), the estimated ice lens density decreased from about 7 to 2 lenses/$m^{-3}$ as the aircraft moved upslope. Near the glacier margin, at lower elevations, more intense summer melt promoted the formation of firn aquifers tens of meters below the surface. One notable example of subsurface characterization beyond the firn layer comes from the Priestley Glacier in East Antarctica, an outlet glacier channeling ice through the Transantarctic Mountains toward the Nansen Ice Shelf (Fig. 4). Outlet glaciers such as this play a critical role in ice discharge from the interior of both the Greenland and Antarctic ice sheets. Along portions of the Priestley Glacier, strong katabatic winds removed surface snow, and extended segments were crevasse-free—ideal conditions for microwave sensing. Motivated by [58], [61], and [62], a combination of airborne radar data at 0.189–0.199 GHz and radiometer measurements from 0.5 to 2 GHz was used to characterize the thermal state and distribution of fresh water at the glacier bed. The presence of basal water was detected based on the spectral signature: specifically, when the TB difference between the 1.980- and 0.540-GHz channels exceeded 10 K. The spatial distribution of inferred water patches is shown in Fig. 4. The selected detection threshold was based on observed spectral evolution along the glacier, from the upstream entrance near site 13 to the terminus on the Nansen Ice Shelf at site 8. Gaps in detected water were interpreted as resulting partly from local crevasse zones, which disrupt the microwave signal. These results support the viability of integrated methods for detecting thermal and hydrological structure at the ice sheet base, even in dynamic or complex terrain. Together, these developments highlight the growing utility of wideband and multisensor microwave approaches for constraining subsurface ice conditions and improving thermomechanical ice sheet models.

*3) Ice Shelves:* Ice shelves are the floating extension of an inland ice sheet over the polar oceans. Located almost exclusively in Antarctica, they play a central role in regulating ice sheet dynamics by buttressing grounded ice, thereby reducing inland ice flow and limiting contributions to sea-level rise. Ice shelves also facilitate the export of glacial meltwater and modulate ocean circulation within subice shelf cavities. Recent mass budget assessments of all Antarctic ice shelves from 1997 to 2021 revealed widespread negative trends [63], [64]. This loss is particularly pronounced in West Antarctica, where basal melting has increased due to intrusions of warm circumpolar deep water. This thinning weakens buttressing capacity and enables acceleration of grounded ice upstream, enhancing mass loss and dynamic imbalance. In the Antarctic Peninsula and other regions, ice shelves are further destabilized by surface processes such as meltwater-driven hydrofracture, as well as by mechanical rift propagation and temperature-dependent weakening in shear margins and suture zones [65], [66].

Ice shelf retreat and collapse are governed by a combination of thermal and structural factors, including rheology, temperature, internal damage, and meltwater content. Temperature plays a particularly important role in rheological behavior: warmer ice deforms more easily, influencing how stress is distributed and accommodated. Meyer and Minchew [67] showed that temperate ice zones, especially in shear margins and suture zones, can act as mechanical weak points that localize strain and contribute to structural weakening. These regions are prone to damage accumulation, enhanced crevassing, and hydrofracture under meltwater loading, all processes that can lead to calving or collapse. Monitoring the thermal structure of ice shelves is, thus, essential for assessing their stability. Low-frequency microwave radiometry offers a unique observational window into subsurface conditions, including englacial temperature and basal composition. However, low-frequency radiometric studies of ice shelves have so far been limited to modeling and single-frequency L-band observations. Using borehole measurements at two locations on the Ross Ice Shelf, Fig. 5 examines the spectral TB response across the 0.5–2-GHz range [68]. At the Little America V site, which consists entirely of meteoric glacial ice, TB increased with frequency. In contrast, at station J-9, where several meters of brine-rich marine ice overlie the ocean, TB decreased with frequency (Fig. 5). The lower frequency signal was enhanced by the higher emissivity of marine ice, increasing sensitivity to the radiometrically cold ocean beneath. This spectral behavior is analogous to that of sea ice growth, where thickness and composition

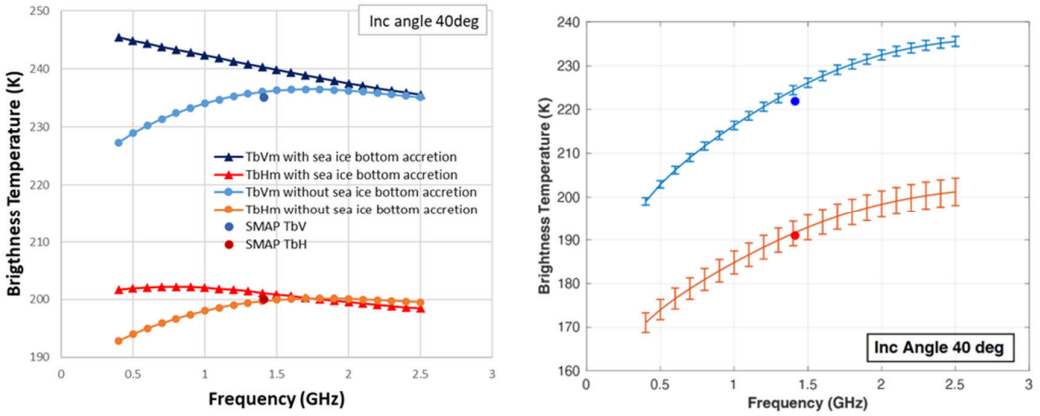


**Fig. 5.** ***Spectral emission of the Ross Ice Shelf (left) at J-9 with marine ice accretion (darker colors) and without (lighter colors), and at Little America V (right), where marine ice is absent. SMAP data are shown as dots [68].***

modulate TB [69]. Thicker shelf ice generally attenuates the signal from the ocean, but the presence of marine ice alters this by increasing basal emissivity, particularly at lower frequencies that are more sensitive to conditions near the ice–ocean interface.

A separate L-band study across the Ross Ice Shelf found a counterintuitive decrease in TB with increasing ice thickness [70], attributed to limited sensing depth (∼500 m) at L band. Thicker ice near the grounding line retained lower temperatures at depth, while thinner shelf ice farther downstream was warmer due to prolonged exposure to basal ocean heat. Additionally, Jezek (personal communication, 2024) suggested that small-scale roughness at the ice–water interface (on the order of millimeters) can further influence the L-band signal by modulating the contribution of the basal layer. Despite promising case studies, current radiometric observations are limited by narrow bandwidths and sparse spatial coverage. Future wideband radiometric systems—operating from ∼0.5 to 2 GHz—could greatly enhance the characterization of basal and englacial temperatures across ice shelves. These observations would provide key constraints for models of ice shelf weakening, fracture propagation, and collapse risk under future climate forcing

## B. Sea Ice

*1) Background:* Long-term changes in sea-ice extent, volume, and mass are key indicators of the climate change impact on the polar regions. Arctic sea ice is not only declining in extent and thinning [71], [72], [73] but is also becoming younger [71], [74], providing clear evidence of climate change [2], [75]. For these reasons, GCOS (2022) recognized sea ice coverage and thickness—key factors in calculating sea-ice volume and mass—as essential climate variables (ECVs) that must be continuously monitored. Moreover, the World Climate Research Program (WCRP) recently recommended further investigation of Antarctic SIT, calling it "the largest single gap in our knowledge of the climate system" [4]. Sea ice processes influence freshwater outflows from melting ice and salinification during ice formation, playing a crucial role in polar ocean freshwater budgets and their variability [83]. Dense, high-salinity water forms primarily over the Arctic and Antarctic continental shelves, where polynyas facilitate sites for continuous sea ice growth [84]. Lateral transport of sea ice also represents a significant surface freshwater flux with major implications for Earth system processes. Tschudi et al. [74] found that reduced Arctic sea ice export through the Fram Strait has increased Greenland Sea salinity, leading to lower sea surface height and stronger cyclonic gyre circulation in the Nordic Seas. This, in turn, enhanced Atlantic Water transport into the Nordic Seas and Arctic Ocean, with the Barents Sea warming linked to weakened ice export [79]. Similarly, the ongoing trends of Southern Ocean surface cooling and freshening have been linked to increased wind-driven northward sea ice transport, which extracts freshwater in the form of sea ice near the Antarctic continent and releases it at the ice edge further north [85]. The weakening of the Atlantic meridional overturning circulation (AMOC) over the past decade has also been associated with Arctic sea ice decline [87], and a reduced efficiency of the "Barents Sea cooling machine" [88], a phenomenon visible as a "cold blob" in the subpolar North Atlantic south of Greenland. Simulations of large-scale sea ice mass balance and upper ocean characteristics are highly sensitive to how ice salinity is represented in ice-ocean models [82]. The lack of large-scale sea ice salinity observations—previously unmeasurable from space—has hindered the ability to validate model parameterizations. Therefore, large-scale observations of sea ice salinity would have a significant impact on verifying model-simulated salinity distributions and assessing the response of high-latitude oceans to ongoing and future climate change. While sea ice concentration has been observed by microwave radiometers since 1972 [83], and drift velocity is currently estimated using both passive

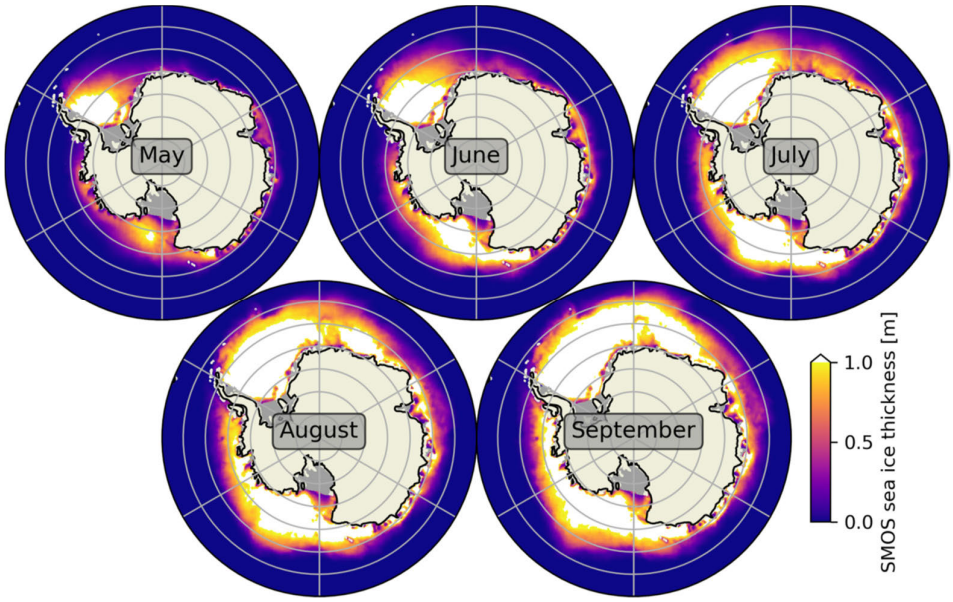


**Fig. 6.** ***Average SMOS SIT (version 3.3) over the time period of 2010–2023 from May to September.***

and active sensors (see [71] and [84]), satellite-based observations of SIT remain challenging (see [85]). The GCOS report recommends improving methodologies for quantifying sea-ice thickness sensing (Action F2—GCOS 2022). The SMOS L-band radiometer has demonstrated the ability to measure SIT for closed-ice thicknesses of less than 50 cm in both the Arctic and Antarctic [13], [18], [86], [87] with the required ECV accuracy (i.e., 10–25 cm [88]).

*2) Microwave Applications:* Several investigators have reported low-frequency airborne radiometer experiments to study the detailed emission process and its sensitivity to arctic ice thickness [89]. Early UHF radiometer measurements over low-salinity Baltic Sea ice showed a nonlinear increase in TB with thickness up to about 1 m, consistent with interference patterns interpreted as coherent emission within the ice layer [90]. Shipborne 611-MHz observations in the Antarctic later confirmed a monotonic emissivity–thickness relationship for first-year ice up to roughly 0.8 m. A semicoherent model introduced random thickness variations to suppress interference effects, yielding a monotonic emissivity–thickness relation that enables inversion for sea-ice thickness [91]. Estimating SIT in the Antarctic presents additional challenges compared to the Arctic, notably due to larger uncertainties in snow cover depth, limited observational coverage, thinner and more dynamic ice, and greater ambiguity in freeboard–to–thickness conversions (see [92]). Sea-ice thickness retrievals from radar and laser altimetry remain limited by uncertainties in snow depth and density, surface roughness, and radar penetration, which together bias freeboard estimates by several centimeters and thickness by up to a few decimeters. These effects are particularly critical for relatively thin, first-year ice, where small freeboard errors translate into large relative thickness uncertainties [85], [93], [94], [95]. Polynyas such as the Ross Sea Polynya are well-delineated. Recognizing these limitations, Kaleschke et al. [96] applied the Arctic thickness retrieval algorithm to the Antarctic (Fig. 6). Ice thicknesses were less than 1 m about the perimeter of the pack, with several validation datasets were available in the Weddell Sea and showed a small mean difference (bias) and an root mean square deviation (RMSD) of about 30 cm between the retrieved and validation data. In a campaign study conducted in 2018, airborne wideband 0.5–2-GHz radiometric measurements were acquired on relatively homogeneous Arctic sea ice in the Lincoln Sea [23], [97]. The study in [96] concludes that the SMOS SIT retrieval algorithm is valid for sea ice up to about 1 m thick. However, for ice thicknesses greater than 1 m, SMOS-based estimates significantly underestimate the thickness compared with in situ observations, due to the limited emission depth at L band. Furthermore, the assumption of fully closed sea ice coverage (100% sea ice concentration) is often not met, leading to a systematic underestimation of SIT, especially in areas of ice divergence, such as within the marginal ice zone.

In a campaign study conducted in 2018, airborne wideband 0.5–2-GHz radiometric measurements were acquired on relatively homogeneous Arctic sea ice in the Lincoln Sea [97]. The results showed spectral variations ranging from 30 K for open water to 20 K for thin ice types, and 10 K for thicker multiyear ice. In that early-fall study, a simple homogeneous ice slab RT model was used to construct lookup tables of modeled spectra parameterized by thickness and salinity. The models were compared to

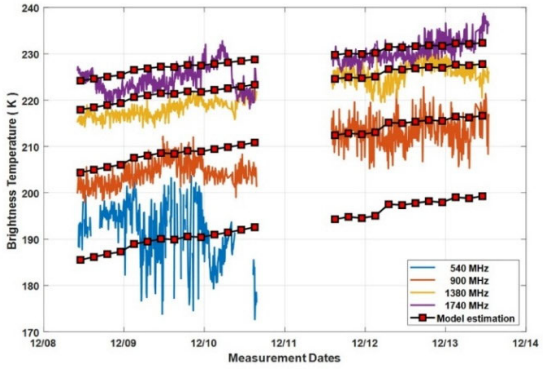


**Fig. 7.** ***Comparison of the measured (thin lines) and modeled (red squares) TB time series for the period when the antenna orientation was kept at 35° off-nadir.***

the measured TB spectra, and the ice thickness and salinity were retrieved by optimization. Retrieved thicknesses ranged between about 0.2 and 2 m for most of the profile, which was not unexpected for the ice pack north of Greenland. Estimated ice salinities varied from about 5 to over 20 ppt, representing overestimates for both multiyear and new ice. The salinity discrepancy may be the result of neglecting important effects, including uncorrected sea ice concentration, physical property gradients through the sea ice, interface roughness, and the presence of snow, along with uncertainties in the electrical properties of the sea ice.

A ground-based ultra-wideband radiometer operating at 0.540, 0.900, 1.380, and 1.740 GHz was later used to measure microwave thermal emissions from an Arctic sea ice floe as part of the Multidisciplinary Drifting Observatory for the Study of Arctic Climate (MOSAiC) Expedition [69]. The instrument was deployed on a drifting ice floe near 86° N, 120° E during December 2019 and observed second-year ice (potentially with refrozen melt ponds) that experienced new ice growth at its base over ten days. Measured TB was compared with the predictions of an RT model for a layered medium consisting of ocean, growing new ice, desalinated remnant second-year ice/refrozen melt pond, and snow layers. Sea ice composition parameters such as time-varying thickness, temperature, and salinity used in the model were determined from in situ measurements; time series of the TBs for the four channels is shown in Fig. 7. The steady increase in TB correlates with the formation of a more emissive layer resulting from the accretion of approximately 10 cm of new ice at the base of the floe.

Insights gleaned from the MOSAiC data were used to model the behavior of wideband radiometry across the Arctic [98]. Simulated Arctic sea-ice thickness and salinity retrievals explored the performance of a nadir-observing microwave radiometer operating with up to 16 frequency channels in the 0.5–2-GHz frequency range.

A simulated TB dataset was produced for Arctic sea ice for the period October 2020–March 2021 using sea-ice thicknesses derived from the SMOS-CryoSat-2 algorithm. Compared to existing sea-ice thickness retrievals obtained from 1.4-GHz microwave radiometers, the results demonstrate that 0.5–2-GHz radiometry can achieve higher sensitivity to a sea-ice thickness within the range 0.5–1.5 m for first-year sea ice and enable the retrieval of multiple sea-ice parameters (thickness and salinity) simultaneously. Fig. 8 reports the main results obtained by this article, demonstrating the capability of a low-frequency wideband microwave radiometer to retrieve SIT and salinity with a retrieval error lower than 20% for thickness and 15% for salinity over the entire season. MOSAiC results were also used in [99] to investigate how brine pocket geometry influences complex permittivity. Based on comparisons of modeled and measured TBs, the authors concluded that the effective permittivity lies between the theoretical spheres and random-needles formulations, consistent with sensitivity analyses and the empirical relationship of Vant et al. [100] although the interpretation remains constrained by measurement uncertainties and model assumptions.

Sea ice observations of Terra Nova Bay, Antarctica, were completed as part of the ISSIUMAX experiment [101] that also collected data on the glaciers and ice sheet of East Antarctica [102]. The UWBRAD 0.5–2-GHz airborne

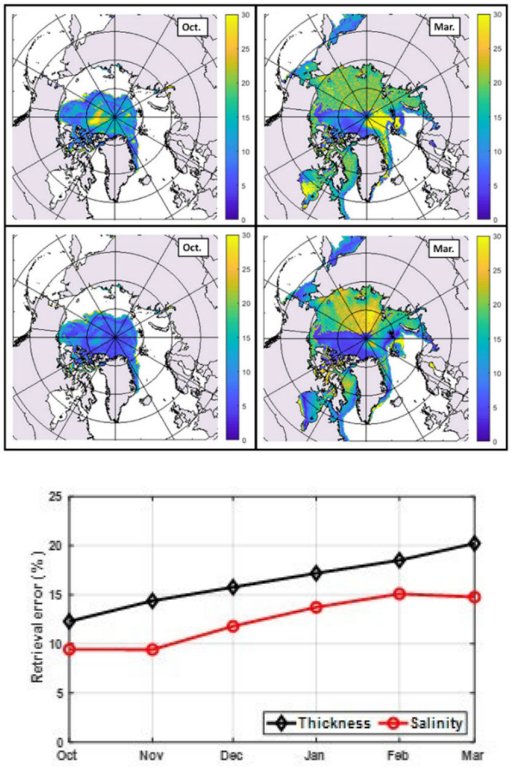


**Fig. 8.** ***Thickness and salinity retrieval error distributions in the Arctic in October and March for thickness (top) and salinity (middle), and the monthly integrated error trend for each sea ice parameter (bottom). The data points correspond to results from the first day of each month [98].***

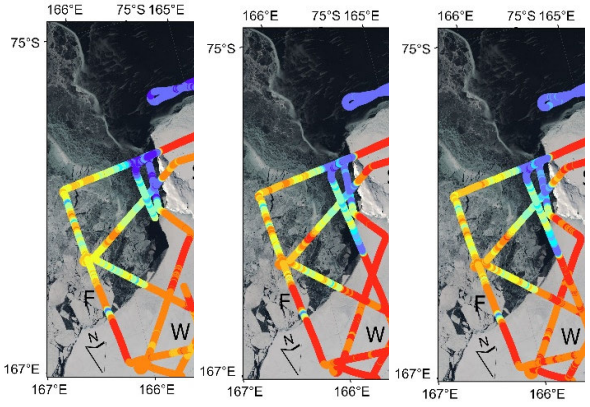


**Fig. 9.** *0.560-(left), 1.370-(center), and 1.950-GHz (right) TB data over Terra Nova Bay sea ice. Note the change in color scale when comparing figures. Locations of Wood Bay (W), Silverfish Bay (S), Gerlache Inlet (G), and Hells Gate (H) are noted. The background map is the Sentinel 3 color composite image collected on November 24, 2018.*

radiometer was flown over the Wood Bay, Silverfish Bay, and Gerlache Inlet portions of Terra Nova Bay during the austral spring of November 2018 (Fig. 9). Several ice types were observed during other studies, including frazil, congelation, fast ice, and platelet ice [103]. An appreciable component (30%) of the total thickness was a subice platelet layer in the vicinity of Silverfish Bay and up to 3-m offshore of Hells Gate Ice Shelf [104]. The thickest subice platelet layer averaged about 3 m thick, and near the Hells Gate Ice Shelf was up to almost 10 m. Although geophysical parameter retrieval is still ongoing, TB maps have shown good empirical correlation with different ice regimes. Fig. 9 shows measured TB at three frequencies (0.560, 1.370, and 1.950 GHz); note that the color scale changes slightly to enhance patterns in the separate images. The TB patterns are similar for all three channels and range from 75 to 260 K; the basal ice growth model predicts a gradual increase of 10 K for all channels. Relatively thick (∼2 m [104], [105]) fast ice in Wood Bay (W) and Silverfish Bay (S) was warmest with a maximum of about 262 K. Thin ice seaward of Wood Bay and either thin ice or open-water seaward of Silverfish Bay and Gerlache Inlet (G) was coolest because of increased contributions from the radiometrically cold ocean. Floes (F in Fig. 9) apparently broken off from the more easterly consolidated ice were warmer (about 235 K). A small lead of new ice is observable between the disconnected floe (F) and the nearby margin of the fast ice in Wood Bay.

In summary, previous studies indicate that low-frequency wideband radiometry has the potential to improve the quantification of sea-ice thickness and volume relative to current capabilities. In the context of CryoRad preparatory studies, described in more detail in Section III, recent analyses based on ECMWF ORAS6 sea-ice fields suggest that a satellite system like CryoRad may be able to resolve the main variability in thickness and volume, potentially within the WMO GCOS uncertainty limits. However, the ability to infer detailed information on sea-ice salinity and surface properties requires further dedicated investigation [106].

### C. Sea Surface Salinity

*1) Background:* SSS is recognized as a key ECV for both the GCOS and the Global Ocean Observing System (GOOS) [107]. At high latitudes, SSS changes control ocean dynamics [108] and result from strong changes in the total freshwater content, with large consequences on the Earth's climate [109], [110] that are very difficult to predict [111]. Particularly, important aspects are the collapse of the AMOC, whose timing could be earlier than predicted by current climate models [112], [113], and the acceleration of Antarctic meltwater discharge, whose impact on Southern Ocean stratification could have important implications on ocean heat and carbon storage, but remains very uncertain [114].

L-band radiometer missions, which mostly operate at the protected band from 1.400 to 1.427 GHz, have provided unprecedented SSS measurements over the global ocean at 40–150-km spatial resolution with a revisit time of three–eight days, and continuity of observations is recognized as a high priority. The current SMOS and SMAP missions have demonstrated the unique information available from remotely sensed SSS, despite their challenges in cold waters. For instance, Grodsky et al. [115] detected interannual variability of SSS in the Chukchi sea concurrent with an anomalous southward shift of the ice edge. Moreover, the seasonal variations in Arctic and Antarctic SSS are consistent with sea ice seasonal cycles [115], [116]. In the Laptev Sea, studies have shown the correlation between low SSS in river plumes, sea surface temperature (SST), and sea ice concentration under the effect of wind, forcing interannual variability [117]. However, the occurrence of these events is very poorly documented due to the limited accuracy of existing observations in cold waters, and their role in the Arctic and Southern Ocean freshwater system remains poorly understood.

Uncertainties of SSS derived from the observation of L-band missions are two–three times larger for cold oceans than for oceans in warm regions [21], [22]. Indeed, weekly SSS error increases in cold polar regions to more than 1 pss as compared to 0.2–0.3 pss for tropical regions. Consequently, the satellite-derived SSS is noisier than the SSS variability in low variability regions such as the Atlantic Subpolar Gyre (Fig. 10). There, the detection of long term SSS trends remains difficult, while SSS is a central element to detect whether this region is tipping, as SSS plays a critical role in controlling ocean surface densities and hence convection [30]. Enhanced accuracy in cold-sea SSS retrievals is, thus, necessary for monitoring interannual to decadal thermohaline variability and sea-level change in polar oceans [118]. Improved observations are also essential for understanding the evolution of the high-latitude

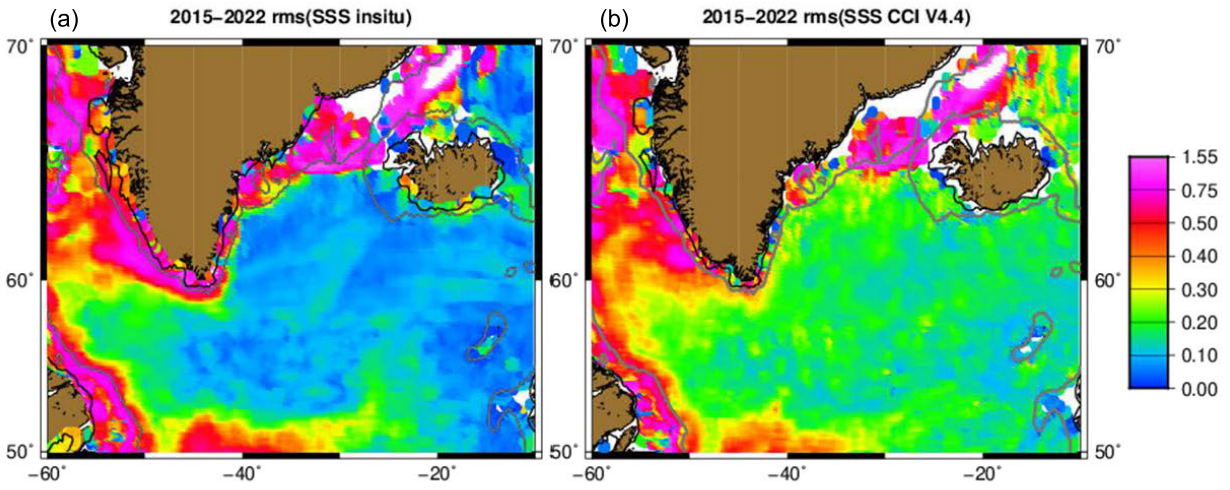


**Fig. 10.** ***Maps of the rms SSS variability as derived from (a) in situ data, October 2015–October 2022, and (b) collocated weekly climate change initiative (CCI) (SMOS + SMAP) SSS fields. The 100- and 500-m bathymetric contours are plotted (thin black line and gray line, respectively). The figure is reproduced from [116].***

freshwater system, including river discharge, precipitation, and sea ice melt/freeze cycles. This is particularly relevant over shallow Arctic shelves, which are hotspots of freshwater exchanges [119]. The current generation of climate models poorly constrains high-latitude water mass properties due to crude representations of physical processes such as lateral mixing (especially in the marginal ice zone), convection, and entrainment. These limitations generate large uncertainties in the modeled response to climate change [111]. SSS simulated with multiple current models without assimilation differs significantly. Fig. 11 shows an illustration on August 5, 2020, of the std of SSS simulated with four reanalysis products from the Copernicus Marine Services. The largest uncertainties are associated with SSS values between 10 and 30 pss (Fig. 11, right).

Polar oceans exhibit a strong coupling between SSS and SIT. Melting ice adds freshwater to the ocean surface, with fresher waters having a higher freezing temperature, promoting an earlier freezing and thicker sea ice [120], [121]. For instance, Zhang et al. [122] evaluated the effect of removing sea ice meltwater and found that SIT in the following freezing season could vary by −43% to +12% depending on ocean stratification. In the Southern Ocean, the recent low sea ice extent state is occurring at a time

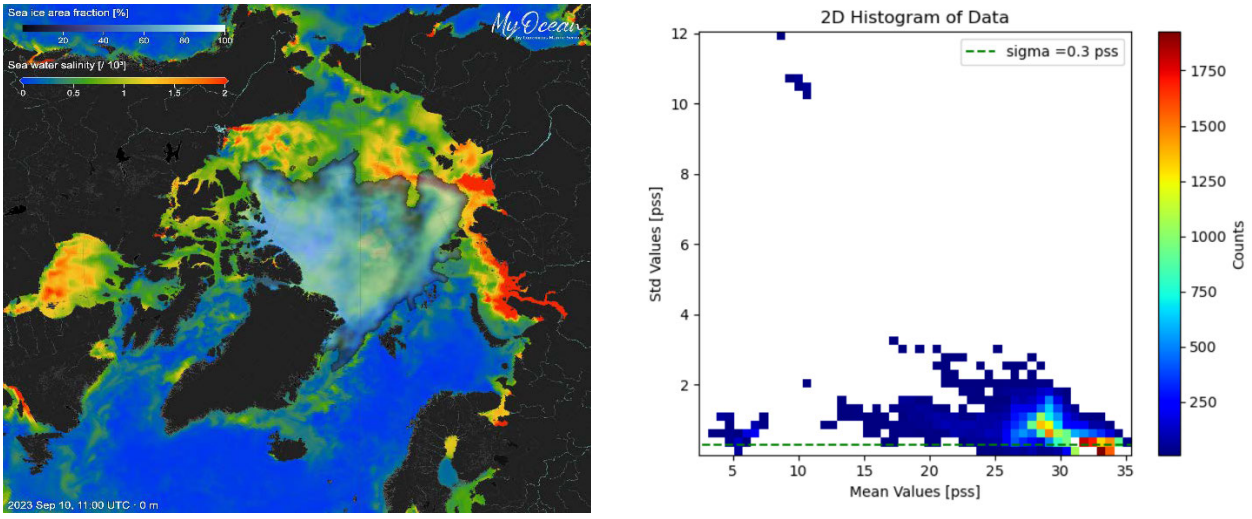


**Fig. 11.** ***STD of SSS simulated with various copernicus marine environment monitoring service (CMEMS) reanalysis products, with sea ice mask (left), and relationship between mean and std (right), units: 0–2 pss. Date: September 2023. The dashed horizontal line indicates the 0.3-pss precision target.***

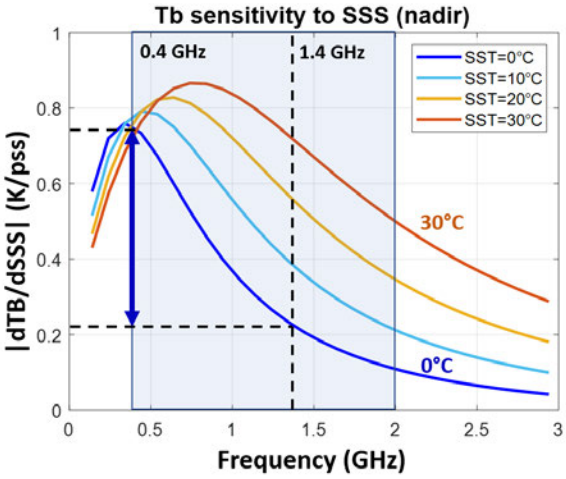


**Fig. 12.** *Absolute value of TB sensitivity to SSS (in $K \cdot pss^{-1}$) as a function of frequency for various SST (SSS is equal to 33 pss). The vertical dashed line shows the operating frequency of L-band missions; the light blue box features the operating frequency of the CryoRad mission, and the horizontal dashed lines show the comparison of the sensitivity of TB to SSS at 0.4 and 1.4 GHz. These sensitivities have been evaluated with [127] (two functions) dielectric constant model.*

when the Antarctic ice sheet and shelf melting is accelerating, and today, the processes governing the coupling between meltwater and sea ice are very uncertain [114]. Moreover, salinity also influences ocean stratification, and preliminary modeling exercises that have included these various processes indicate that the SSS impact on sea ice formation varies depending on regions and time.

*2) Microwave Applications:* In cold water, the sensitivity of TB to SSS is a factor of three larger at 0.4 GHz than at 1.4 GHz (Fig. 12). Hence, SSS retrieval from a 0.4 to 2 GHz wideband radiometer should be improved, due to the larger sensitivity of the low part of this wideband frequency to SSS [123]. The sensitivity of TB to SST is also larger at very low frequency, but the wide frequency band could add a constraint on both SSS and SST [124].

Accurate retrieval of SSS depends on the accuracy of the RT modeling over the wideband frequencies, with TB sensitivity to SSS driven by the sea water permittivity model. Recent models developed from L-band measurements have been shown to be compatible with recent P-band (0.700 GHz) laboratory measurements to the first order [125]. According to theoretical sea surface emissivity models, contributions of sea surface roughness and foam to sea surface TB are expected to decrease with decreasing frequencies [124], but their precise contributions at frequencies lower than 1.4 GHz need to be validated, especially since parametrization of theoretical foam modeling at low frequencies remains difficult [126]. In addition, galactic signal, sun emission, and Faraday rotation greatly increase at low frequency, and their contributions will need to be treated with great care [23].

In the context of CryoRad preparatory studies, simulations have been performed to estimate uncertainties on retrieved SSS from a wideband radiometer using a Bayesian approach to retrieve SSS, SST, and wind speed. A few preliminary results are presented in the following. A simplified direct model and the same radiometric noise in 100-MHz frequency bands spread between 0.4 and 2 GHz have been considered. The simplified direct model, as in [123], takes only the contribution of sea surface emissivity to TB into account.

The dielectric constant model is the two-function model from [127], consistent with recent laboratory P-band measurements [125], while the wind impact is parametrized similarly to [123]. SST and wind speed are assumed to be known a priori, with uncertainties of 0.3 °C and $1\ m \cdot s^{-1}$, respectively, as could be expected when CIMR observations are available. For "common" polar ocean conditions (SSS = 33 pss and SST = 0 °C), the SSS uncertainty reaches 0.3 pss for a radiometric noise (NeDT, taken here at 150 K) of 0.35 K (Fig. 13). This is an order of magnitude lower than what can be achieved with an L-band radiometer (Fig. 14). The reduction of SSS uncertainties is even stronger at low to moderate SSS, as the uncertainty obtained with a wideband radiometer (0.2 pss at SSS = 15 pss and SST = 2 °C) is ten times lower than with a single L-band frequency radiometer. Actually, at very low frequency, the sensitivity of TB to SSS increases with decreasing SSS, whereas at L band, it decreases. This property is particularly noteworthy because the greatest discrepancies between SSS simulated by different models are found in regions with low SSS values (Fig. 10).

## D. Other Applications (Soil Moisture and Vegetation)

*1) Background:* While the previous sections have pointed out the potential of low-frequency microwave

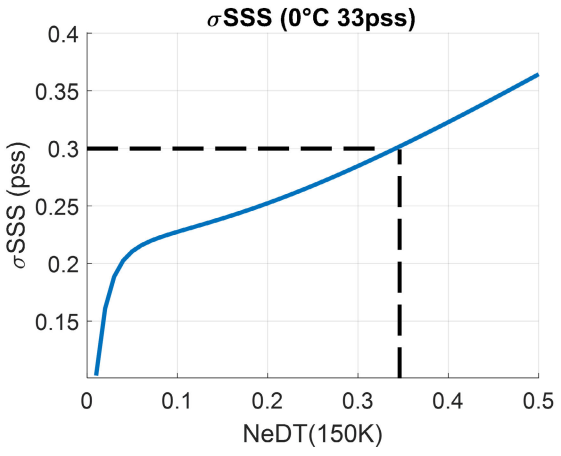


**Fig. 13.** *SSS uncertainties simulated as a function of radiometric noise at 150 K (moderate wind speed is equal to 8 $m \cdot s^{-1}$).*

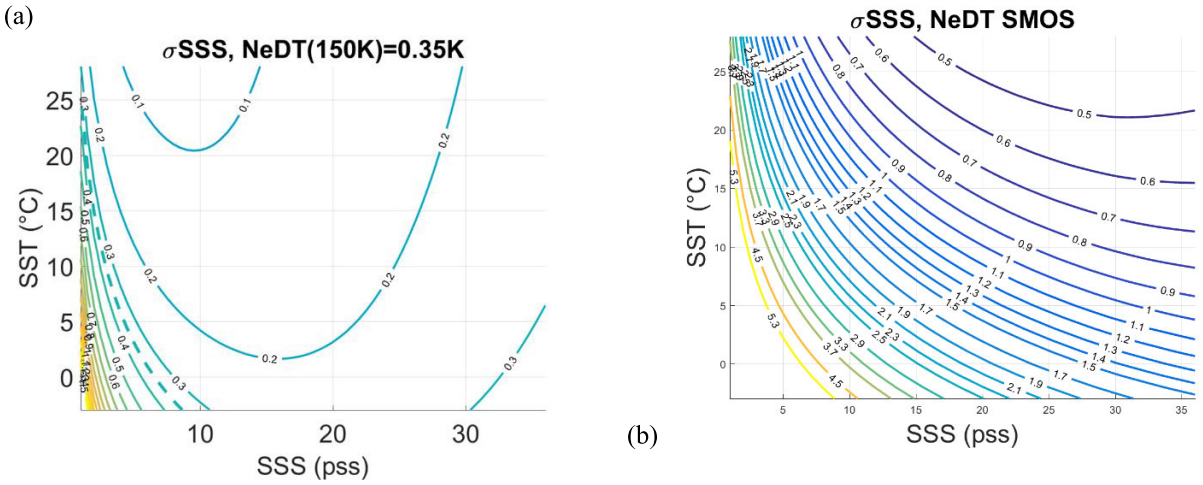


**Fig. 14.** *SSS random uncertainty as a function of SSS and SST, assuming a 0.3 °C random uncertainty on SST and 1-m · s$^{-1}$ random uncertainty on wind speed for (a) 0.4–2-GHz wideband radiometer with a radiometric noise of 0.35 K and (b) L-band radiometer, having the same radiometric noise and incidence angles as SMOS, center of the swath.*

observations in polar regions, they can also provide relevant information on ocean and land surface states at global scales. L-band measurements from SMOS and SMAP have already demonstrated their capability in monitoring soil moisture and vegetation biomass, which are key elements of the water and carbon cycles [128]. The surface soil moisture products derived from the SMOS and SMAP missions have been extensively studied and proven to be well correlated to in situ measurements [129], [130] and will continue to be developed (e.g., drought conditions and soil moisture for vegetation in the root zone). However, L-band observations are typically limited to the top few centimeters of soil (approximately 5 cm [131]) and can be substantially affected by surface roughness [132] and vegetation cover [133], especially in forested and agricultural regions. Microwave radiometry monitors vegetation states and dynamics via the retrieved vegetation optical depth (VOD) parameter, which is a variable that quantifies the total attenuation of microwave when it passes through the canopy. The derived VOD parameter at L/C bands is related to the vegetation water content (VWC, kg/m$^2$), but it has further been shown to be a good proxy for above-ground biomass (AGB) [134], [135] and to the tree height [136]. More than 12 years of SMOS observations have shown the evolution of AGB and more importantly of carbon stocks, as both sources and sinks [137], [138], [139]. However, studies have shown that L-VOD saturates at an AGB threshold of 300–400 Mg/ha [135], [137], whereas dense forests, such as tropical rainforests or Pacific temperate rainforests (located at latitudes above 40°S and 40°N), can exhibit AGB values exceeding 500 Mg/ha, and in some cases reaching up to 3000 Mg/ha.

Given the crucial role of these dense forests in regulating the global carbon cycle, biodiversity, and climate, this underscores the strong need for microwave radiometry at frequencies lower than L band, which will provide more reliable estimates of AGB in ecosystems where L-band signals saturate [140]. Furthermore, methods based on neural networks have further shown the potential to estimate the AGB [141] with greater accuracy than through the VOD, presenting important advantages for including the multifrequency capability of future missions. For many years, the potential advantages of lower frequencies (i.e., P-band radiometry in the range of 0.3–1 GHz) were largely theoretical, due to the lack of observational data. More recently, Monash University, Australia, has led efforts to provide observational evidence through a series of comprehensive field experiments (i.e., PRISM https://www.prism.monash.edu and APPLEX campaigns https://www.applex.monash.edu). These initiatives have yielded invaluable datasets and significantly advanced the understanding and application of P-band radiometry, which are summarized hereafter.

*2) Microwave Application:*

*a) Surface SMC retrieval:* It was demonstrated by Shen et al. [142] that the P band has a deeper soil moisture sensing depth (∼7 cm at 0.75 GHz) than the L band (∼5 cm at 1.4 GHz) while maintaining similar correlation, or alternatively, providing higher accuracy at the same 5 cm depth. This deeper sensing depth, attributed to its longer wavelength, is further supported by modeling results that indicated the potential for a sensing depth of over 10 cm at frequencies below 0.5 GHz [142].

P band has also shown a reduced sensitivity to surface roughness compared to shorter wavelengths. While very smooth surfaces (i.e., root mean square (rms) height of ∼0.8 cm) affect both L and P bands minimally, P band performed better under rougher conditions (i.e., rms height of ∼1.6 cm). This robustness is particularly important

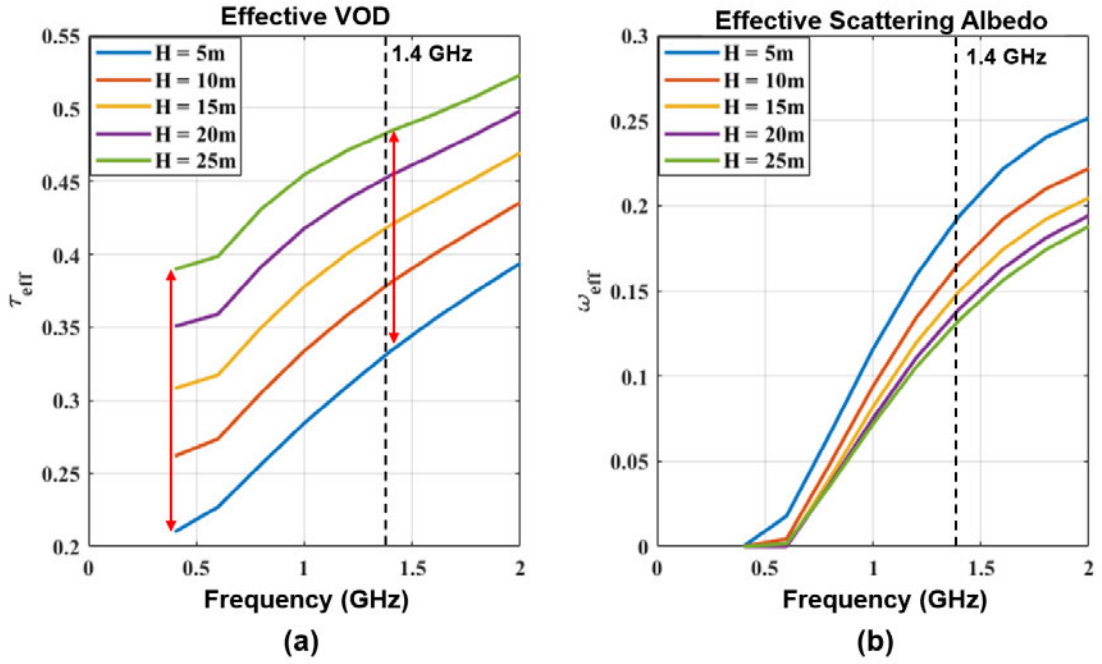


**Fig. 15.** ***Effective RT properties simulated by MEMLV. (a) Effective VOD from 0.4 to 2 GHz. (b) Effective scattering albedo from 0.4 to 2 GHz, for canopy height varying from 5 to 25 m. The figure is reproduced from [148].***

in agricultural landscapes with structured row patterns. In such scenarios, P-band retrievals (unbiased rms error (ubRMSE) of ∼0.01–0.02 $m^3/m^3$) outperformed L-band retrievals (ubRMSE of ∼0.03–0.04 $m^3/m^3$), indicating that P band may require less stringent discrimination of tilled surfaces for accurate soil moisture content (SMC) estimation [143].

*b) SMP retrieval using multifrequency synergy:* Understanding the vertical distribution of SMC, particularly within the root zone, is crucial for applications such as agricultural water management and land–atmosphere interaction studies (see [144]). While L band provides limited insight into the moisture of deeper soil layers, combining L- and P-band observations allows for depth-resolved profile retrieval. The inherently deeper sensing depth of P band complements L band, with their joint use enabling the emissions from different soil layers to be disentangled. Inversions have typically involved fitting a parameterized function (e.g., a polynomial) [145], representing the profile shape to the combined TB observations using an RT model. A recent comparison of emission models and profile representations [146], [147] suggests that while coherent models offer slight improvements in the TB prediction under bare soil conditions, the more simplistic incoherent models performed comparably in vegetated environments and so are preferable when considering computational efficiency.

Using combined L- and P-band data, a coherent modeling approach and a second-order polynomial soil moisture profile (SMP) shape assumption; it was shown that the SMP variation could be estimated for depths up to 28 cm with an RMSE of 0.04 $m^3/m^3$ during dry periods [149]. Notably, a follow-up study by Kerr et al. [129] showed that a uniform incoherent model, combined with the same polynomial profile, produced similar RMSEs across different land covers and depths: ∼0.03 (0–5 cm), ∼0.08 (0–30 cm), and ∼0.1 $m^3/m^3$ (0–60 cm).

*c) Vegetation optical depth:* For vegetated areas, the P band demonstrated improved performance compared to the L band. A recently developed wideband RT model, named the microwave emission model for layer vegetation (MEMLV) [148], demonstrates the advantages of P-band radiometry in the application of coniferous forest. The MEMLV models the canopy upwelling TB by treating the coniferous canopy as a multilayer structure that accounts for both canopy architecture (e.g., height and gap fraction) and the properties of its constituents (e.g., size, orientation, and number density). The effective VOD and scattering albedo (an important parameter in VOD retrieval that accounts for the fraction of scattering in total attenuation) are then derived by minimizing the cost function between the TB simulated with the single-layer two-stream model [150] and that simulated with MEMLV.

Fig. 15 presents an example of the modeled effective VOD and scattering albedo from P to L band using the developed MEMLV. It is seen that the effective VOD is almost doubled at P band when the canopy height changes from 5 to 25 m, while at L band, it only increases by 50%. The increased dynamics significantly support the accuracy of the retrieved VOD. On the other hand, Fig. 15(b) shows that the effective scattering albedo at P band is

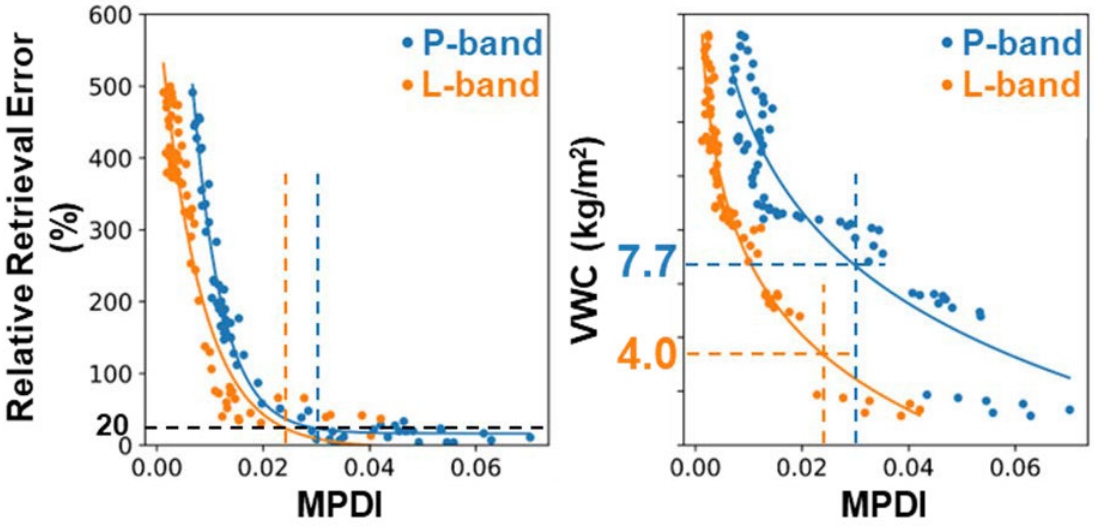


**Fig. 16.** ***Relationship between relative retrieval error and the VWC established through the microwave polarization difference index (MPDI) [151].***

almost zero, while it varies from 0.1 to 0.2 at L band, depending on the canopy height. The parameterization of the scattering albedo is always a challenge in the VOD retrieval algorithm, which strongly affects the retrieved VOD. One of the advantages of using P band in VOD retrieval is that the scattering albedo can be negligible, which will significantly simplify the retrieval process. Furthermore, the wideband capability provided by future missions, such as the CryoRad mission, will help to detect the vegetation property at different depths (or layers) within the canopy, providing an unprecedented opportunity to further understand the phenology and biology of dense forests.

Since VOD at P band is, in general, lower than L band, a higher VWC threshold can be achieved for reliable SMC retrieval with P band ($\sim$7.7 kg/m$^2$) compared to L band ($\sim$4.0 kg/m$^2$), as shown in Fig. 16. For instance, under low-to-moderate VWC conditions, such as in wheat canopies (VWC $<$ 4 kg/m$^2$), P band was able to achieve acceptable accuracy even without accounting for vegetation effects in the retrieval model [151]. The advantages of P band were shown to be even more pronounced in dense vegetation. In studies involving corn canopies with VWC up to $\sim$20 kg/m$^2$, P-band retrievals showed lower RMSEs ($\sim$0.054–0.074 m$^3$/m$^3$) compared to L-band retrievals, which often exceeded 0.1 m$^3$/m$^3$ [125]. Across these scenarios, the relationship between VOD and VWC (for VWC ranging from 0 to 20 kg/m$^2$) was found to be logarithmic for both bands. P band enabled a more robust VOD retrieval due to the additional information captured in its dual-polarized TB observations. Furthermore, vegetation parameters calibrated for P-band RT models showed better transferability across conditions compared to those for L band [152], [153].

## III. SPACEBORNE MISSION CONCEPTS

The previous sections demonstrate that 0.4–2-GHz radiometers can improve existing satellite products, and in particular, attribute to their significantly enhanced emission depth and the capability of sensing the geophysical properties at different depths. Additionally, by using this technique, it is possible to obtain new products that were not anticipated in current or upcoming spaceborne missions. Based on these insights, an international consortium has proposed the deployment of 0.4–2-GHz radiometers in space. Two mission concepts are discussed here.

### A. CryoRad Mission Concept

The CryoRad mission [154] was designated by ESA in 2019 as a “commended” mission in the Earth Explorer 11 competition and was selected in 2024 as one of the four candidates for the Earth Explorer 12 (EE12) program. The CryoRad mission is proposed to be launched in the 2036 timeframe in case of final selection as the next EE12, based on a cost at completion (CaC) not exceeding 550 M€(e.c. 2022). After completion of Phase-0 activities, and following a User Consultation Meeting (UCM) planned in mid 2026, two mission concepts will be selected by ESA to proceed to Phase-A study activities. Thereafter, one of the concepts will be selected for implementation and will enter Phase B in 2028. The CryoRad mission consists of a single satellite hosting a 0.4–2-GHz wideband radiometer payload. Two industrial studies to define the

**Table 1** CryoRad Products

| Product | Spatial Resolution | Temporal Resolution | Accuracy | Latency |
|---|---|---|---|---|
| Ice sheet temperature Profile and Basal state | Better than 50 km (Goal 25 km) | Better than 6 months | Better than 1.5 K at the base/ better than 1 K in the first 2000 m | Better than 6 months |
| Sea Surface Salinity | Better than 50 km (Goal 25 km) | Better than 7 days (Goal 3 days) | Better than 0.2-0.4 pss (Goal 0.1 pss) for SST from -3 to 20°C | 12 hours |
| Sea Ice Thickness (SIT) and Salinity (SIS) | Better than 50 km (Goal 25 km) | Better than 1 month (Goal Weekly). | SIT: better than 20% error for SIT from 0 to 100 cm. SIS: better than 20% error for SIT from 0 to 300 cm. | 12 hours |

mission technical characteristics meeting mission scientific requirements began in early 2025. The plan is to arrive at the UCM with two solid proposals demonstrating the mission feasibility in terms of cost and scientific requirements. Ongoing industrial studies are considering the following requirements.

*1) Spatial and Temporal Coverage/Resolution:* The instrument will provide contiguous and complete coverage of our planet and with a maximum revisit time of ten days for latitudes higher than 50°, *without* any observational gaps at the poles. The spatial resolution, at product level L1B, will be better than 15 km at 1.4 GHz (i.e., the reference frequency for existing L-band missions) and better than 50 km at 0.4 GHz.

*2) System Characteristics and Performance:* The instrument will acquire the TB of the upwelling microwave radiation over the full instantaneous 0.4–2-GHz bandwidth over all Earth surfaces in subbands of 100 MHz or less. In the protected band (1.4–1.425 GHz), a resolution of 25 MHz is expected. To detect potential RFI contamination, a native spectral resolution better than 1 MHz is expected [155]. The total standard uncertainty (TSU) is required to be $<$0.35 K over one sample of the full spectral range (1-sigma, 100-MHz bandwidth) to fit with the objective of the primary mission products. This TSU includes components having individual requirements: NE$\Delta$T, end-to-end lifetime radiometric stability, orbital stability, and a bias (e.g., associated with prelaunch characterization uncertainty). Having these characteristics, it is expected that the mission will provide the innovative products described in Table 1.

The payload addresses the EE12 scientific requirements by keeping a simple architecture that makes the mission credible and compatible in terms of cost and planning, while meeting the scientific goals. CryoRad will be designed to observe at near-nadir in a single circular polarization, which mitigates the effects of Faraday rotation as well as the degradations in spatial resolution that occur for oblique incidence geometries. Preliminary studies [154], [156] point out that the antenna system will be composed of a large deployable reflector (LDR) of around 10 m diameter illuminated by an array of feeds, which can cover the complete frequency range and provide different spatial resolutions depending on the frequency, i.e., finer at higher frequencies and coarser at lower frequencies. The type/number of feeds, the orbit type and altitude, and the consequent swath width will be designed to meet the abovementioned requirements.

### B. PolarRad Mission Concept

PolarRad is a mission concept similar to the CryoRad for sensing polar regions using a wideband radiometer operating from 0.5 to 2 GHz. Initial formulation studies were conducted in 2020–2021 for the PolarRad wideband radiometer instrument. PolarRad was targeted for NASA's Earth Ventures-Instruments (EV-I) Program, but changes to the EV-I Program cost cap in 2021 made the concept unsuitable for further EV-I proposal development. Like the CryoRad initial concept, PolarRad would also observe at nadir in a single circular polarization, to provide improved measurements of ice sheet internal temperatures, ocean salinity, SIT, and sea ice salinity, among other scientific products. Unlike CryoRad, PolarRad would retain a single 50-km spatial resolution for all frequency channels in order to reduce cost by avoiding the use of multiple spatial footprints for the instrument's higher frequencies (for example, 2 GHz). While this would result in some loss of science information otherwise available from the finer resolution measurements, many of the primary science goals are retained, albeit at a uniform 50-km spatial resolution. Development of the PolarRad mission concept is expected to continue when suitable NASA Earth Ventures class opportunities become available.

## IV. CONCLUSION

This article has discussed how wideband low microwave frequency radiometers from P to S band can be used to

measure and monitor key variables, which are now poorly known, to contribute to a better understanding of Earth processes and future trends. In particular, microwave radiometry at these frequencies demonstrates an increased sensing depth in soil, sea ice, and land ice, allowing a better characterization of soil moisture, a better estimate of SIT in the 0–1-m range, and improved capabilities to measure the ice sheet temperature profile with respect to existing satellite missions. The low frequencies also exhibit an enhanced sensitivity to SSS and enable the SSS uncertainty in cold water to be reduced. The need for these measurements is justified by contributions to: 1) understanding and quantification of the freshwater cycle and water mass formation at high latitudes; 2) understanding ice sheets and shelves dynamics followed by quantification of their contribution to global sea-level rise; 3) understanding and monitoring of sea ice dynamics in polar regions; and 4) better characterization of soil and vegetation properties to better assess their impact on water and carbon cycles. These advantages motivate ongoing efforts in multiple countries to investigate theoretical and modeling aspects, collect additional datasets through airborne and ground-based campaigns, and conduct industrial studies for space mission implementation.

## Acknowledgment

**Giovanni Macelloni**, **Marco Brogioni**, and **Marion Leduc-Leballeur** are with the Institute of Applied Physics "Nello Carrara" in National Research Council, 50019 Sesto Fiorentino, Italy (e-mail: giovanni.macelloni@cnr.it; marco.brogioni@cnr.it; marion.leduc-leballeur@cnr.it).
**Kenneth C. Jezek** and **Joel T. Johnson** are with The Ohio State University, Columbus, OH 43210 USA (e-mail: jezek51@gmail.com; johnson.1374@osu.edu).
**Ghislain Picard** and **Ange Haddjeri** are with Universitè Grenoble Alpes, 38400 Saint-Martin-d'Hères, France (e-mail: ghislain.picard@univ-grenoble-alpes.fr; ange.haddjeri@univ-grenoble-alpes.fr).
**Lars Kaleschke** is with the Alfred Wegener Institute, 27515 Bremerhaven, Germany (e-mail: lars.kaleschke@awi.de).
**Jacqueline Boutin** is with the Laboratoire d'Océanographie et du Climat-Expérimentations et Approches Numériques, 75005 Paris, France (e-mail: jacqueline.boutin@locean.ipsl.fr).
**Jean Luc Vergely** is with the ACRI-ST, 78280 Guyancourt, France (email: jean-luc.vergely@acri-st.fr).
**Nicolas Kolodziejczyk** is with the University of Brest, CNRS, Ifremer, IRD, Laboratoire d'Océanographie Physique et Spatiale (LOPS), IUEM, 29280 Plouzané, France (e-mail: nicolas.kolodziejczyk@univ-brest.fr).
**Laurent Bertino** is with the Nansen Environmental and Remote Sensing Center, 5007 Bergen, Norway (e-mail: Laurent.Bertino@nersc.no).
**Emmanuel P. Dinnat** is with the Cryospheric Sciences Laboratory, NASA Goddard Space Flight Center, Greenbelt, MD 20771 USA (e-mail: emmanuel.dinnat@nasa.gov).
**Rasmus T. Tonboe** is with the Technical University of Denmark, 2800 Kongens Lyngby, Denmark (e-mail: rtato@dtu.dk).
**Anne Munck Solgaard** and **Synne Høyer Svendsen** are with the Geological Survey of Denmark and Greenland, 1350 Copenhagen, Denmark (e-mail: aso@geus.dk; syhsv@geus.dk).
**Xiaoji Shen** is with the College of Surveying and Geo-Informatics, Tongji University, Shanghai 200092, China (e-mail: xiaoji_shen@tongji.edu.cn).
**Jeffrey P. Walker** is with the University of Monash, Clayton, VIC 3800, Australia (e-mail: Jeff.Walker@monash.edu).
**Stef Lhermitte** is with Katholieke Universiteit Leuven, 3000 Leuven, Belgium (e-mail: stef.lhermitte@kuleuven.be).
**Yiwen Zhou** is with the Swiss Federal Institute for Forest, Snow and Landscape Research (WSL), 8903 Birmensdorf, Switzerland (e-mail: yiwen.zhou@wsl.ch). ■

## REFERENCES

[1] T. Frederikse et al., "The causes of sea-level rise since 1900," *Nature*, vol. 584, no. 7821, pp. 393–397, Aug. 2020, doi: 10.1038/s41586-020-2591-3.
[2] *The Ocean and Cryosphere in a Changing Climate: Special Report of the Intergovernmental Panel on Climate Change*, 1st ed., Cambridge, U.K.: Cambridge Univ. Press, 2022, doi: 10.1017/9781009157964.
[3] J. Stroeve and D. Notz, "Changing state of Arctic sea ice across all seasons," *Environ. Res. Lett.*, vol. 13, no. 10, Sep. 2018, Art. no. 103001, doi: 10.1088/1748-9326/aade56.
[4] M. J. Siegert et al., "Antarctic extreme events," *Frontiers Environ. Sci.*, vol. 11, Aug. 2023, Art. no. 1229283, doi: 10.3389/fenvs.2023.1229283.
[5] R. L. Thoman et al., "The Arctic," *Bull. Amer. Meteorological Soc.*, vol. 103, no. 8, pp. S257–S306, Aug. 2022, doi: 10.1175/bams-d-22-0082.1.
[6] R. G. Williams et al., "Asymmetries in the southern ocean contribution to global heat and carbon uptake," *Nature Climate Change*, vol. 14, no. 8, pp. 823–831, Aug. 2024, doi: 10.1038/s41558-024-02066-3.
[7] L. Cheng, K. E. Trenberth, J. Fasullo, T. Boyer, J. Abraham, and J. Zhu, "Improved estimates of ocean heat content from 1960 to 2015," *Sci. Adv.*, vol. 3, no. 3, Mar. 2017, Art. no. 1601545, doi: 10.1126/sciadv.1601545.
[8] I.-H. Park, S.-W. Yeh, W. Cai, G. Wang, S.-K. Min, and S.-K. Lee, "Present-day North Atlantic salinity constrains future warming of the Northern Hemisphere," *Nature Climate Change*, vol. 13, no. 8, pp. 816–822, Aug. 2023, doi: 10.1038/s41558-023-01728-y.
[9] D. I. A. McKay et al., "Exceeding 1.5°C global warming could trigger multiple climate tipping points," *Science*, vol. 377, no. 6611, p. 7950, Sep. 2022, doi: 10.1126/science.abn7950.
[10] S. Abdalla et al., "Altimetry for the future: Building on 25 years of progress," *Adv. Space Res.*, vol. 68, no. 2, pp. 319–363, Jul. 2021, doi: 10.1016/j.asr.2021.01.022.
[11] G. Macelloni, M. Leduc-Leballeur, M. Brogioni, C. Ritz, and G. Picard, "Analyzing and modeling the SMOS spatial variations in the east Antarctic Plateau," *Remote Sens. Environ.*, vol. 180, pp. 193–204, Jul. 2016, doi: 10.1016/j.rse.2016.02.037.
[12] G. Macelloni, M. Leduc-Leballeur, F. Montomoli, M. Brogioni, C. Ritz, and G. Picard, "On the retrieval of internal temperature of Antarctica ice sheet by using SMOS observations," *Remote Sens. Environ.*, vol. 233, Nov. 2019, Art. no. 111405, doi: 10.1016/j.rse.2019.111405.
[13] L. Kaleschke, X. Tian-Kunze, N. Maaß, M. Mäkynen, and M. Drusch, "Sea ice thickness retrieval from SMOS brightness temperatures during the Arctic freeze-up period," *Geophys. Res. Lett.*, vol. 39, no. 5, p. 2012, Mar. 2012, doi: 10.1029/2012gl050916.
[14] K. Rautiainen et al., "SMOS prototype algorithm for detecting autumn soil freezing," *Remote Sens. Environ.*, vol. 180, pp. 346–360, Jul. 2016, doi: 10.1016/j.rse.2016.01.012.
[15] J. Ortet et al., "Retrieving frozen ground surface temperature under the snowpack in the Arctic permafrost area from SMOS observations," *Cryosphere*, vol. 19, no. 9, pp. 3571–3598, Sep. 2025, doi: 10.5194/tc-19-3571-2025.
[16] A. Colliander, M. Mousavi, J. S. Kimball, J. Z. Miller, and M. Burgin, "Spatial and temporal differences in surface and subsurface meltwater distribution over Greenland ice sheet using multi-frequency passive microwave observations," *Remote Sens. Environ.*, vol. 295, Sep. 2023, Art. no. 113705, doi: 10.1016/j.rse.2023.113705.
[17] L. Kaleschke, X. Tian-Kunze, N. Maas, R. Ricker, S. Hendricks, and M. Drusch, "Improved retrieval of sea ice thickness from SMOS and CryoSat-2," in *Proc. IEEE Int. Geosci. Remote Sens. Symp. (IGARSS)*, Jul. 2015, pp. 5232–5235.
[18] L. Kaleschke, N. Maaß, C. Haas, S. Hendricks, G. Heygster, and R. T. Tonboe, "A sea-ice thickness retrieval model for 1.4 GHz radiometry and application to airborne measurements over low salinity sea-ice," *Cryosphere*, vol. 4, no. 4, pp. 583–592, Dec. 2010, doi: 10.5194/tc-4-583-2010.
[19] N. Reul et al., "Sea surface salinity estimates from spaceborne L-band radiometers: An overview of the first decade of observation (2010–2019)," *Remote Sens. Environ.*, vol. 242, Jun. 2020, Art. no. 111769, doi: 10.1016/j.rse.2020.111769.
[20] N. Vinogradova et al., "Satellite salinity observing system: Recent discoveries and the way forward," *Frontiers Mar. Sci.*, vol. 6, p. 243, May 2019, doi: 10.3389/fmars.2019.00243.
[21] W. Tang et al., "The potential and challenges of using soil moisture active passive (SMAP) sea surface salinity to monitor Arctic ocean freshwater changes," *Remote Sens.*, vol. 10, no. 6, p. 869, Jun. 2018, doi: 10.3390/rs10060869.
[22] A. Supply et al., "New insights into SMOS sea surface salinity retrievals in the Arctic ocean," *Remote Sens. Environ.*, vol. 249, Nov. 2020, Art. no. 112027, doi: 10.1016/j.rse.2020.112027.
[23] J. T. Johnson et al., "Microwave radiometry at frequencies from 500 to 1400 MHz: An emerging technology for Earth observations," *IEEE J. Sel. Topics Appl. Earth Observ. Remote Sens.*, vol. 14, pp. 4894–4914, 2021, doi: 10.1109/JSTARS.2021.3073286.
[24] M. J. Andrews, J. T. Johnson, M. Brogioni, G. Macelloni, and K. C. Jezek, "Properties of the 500–2000-MHz RFI environment observed in high-latitude airborne radiometer measurements," *IEEE Trans. Geosci. Remote Sens.*, vol. 60, 2022, Art. no. 5301311, doi: 10.1109/TGRS.2021.3090945.
[25] T. L. Edwards et al., "Projected land ice contributions to twenty-first-century sea level rise," *Nature*, vol. 593, no. 7857, pp. 74–82, May 2021, doi: 10.1038/s41586-021-03302-y.
[26] A. Wernecke, T. L. Edwards, I. J. Nias, P. B. Holden, and N. R. Edwards, "Spatial probabilistic calibration of a high-resolution Amundsen sea

embayment ice sheet model with satellite altimeter data," *Cryosphere*, vol. 14, no. 5, pp. 1459–1474, May 2020, doi: 10.5194/tc-14-1459-2020.

[27] H. Goelzer et al., "The future sea-level contribution of the Greenland ice sheet: A multi-model ensemble study of ISMIP6," *Cryosphere*, vol. 14, no. 9, pp. 3071–3096, Sep. 2020, doi: 10.5194/tc-14-3071-2020.

[28] H. Seroussi et al., "ISMIP6 Antarctica: A multi-model ensemble of the Antarctic ice sheet evolution over the 21st century," *Cryosphere*, vol. 14, no. 9, pp. 3033–3070, Sep. 2020, doi: 10.5194/tc-14-3033-2020.

[29] M. Mellor and R. Testa, "Effect of temperature on the creep of ice," *J. Glaciology*, vol. 8, no. 52, pp. 131–145, 1969, doi: 10.3189/s0022143000020803.

[30] K. M. Cuffey and G. D. Clow, "Temperature profile of the west antarctic ice sheet divide deep borehole," U.S. Antarctic Program (USAP) Data Center, 2014, doi: 10.7265/N5V69GJW.

[31] A. Løkkegaard et al., "Greenland and Canadian Arctic ice temperature profiles database," *Cryosphere*, vol. 17, no. 9, pp. 3829–3845, Sep. 2023, doi: 10.5194/tc-17-3829-2023.

[32] B. S. Lecavalier et al., "Antarctic ice sheet paleo-constraint database," *Earth Syst. Sci. Data*, vol. 15, no. 8, pp. 3573–3596, Aug. 2023, doi: 10.5194/essd-15-3573-2023.

[33] J. A. MacGregor et al., "GBaTSv2: A revised synthesis of the likely basal thermal state of the Greenland ice sheet," *Cryosphere*, vol. 16, no. 8, pp. 3033–3049, Aug. 2022, doi: 10.5194/tc-16-3033-2022.

[34] T. Zhang et al., "Evaluating different geothermal heat-flow maps as basal boundary conditions during spin-up of the Greenland ice sheet," *Cryosphere*, vol. 18, no. 1, pp. 387–402, Jan. 2024, doi: 10.5194/tc-18-387-2024.

[35] M. Leduc-Leballeur, G. Picard, G. Macelloni, A. Mialon, and Y. H. Kerr, "Melt in Antarctica derived from Soil Moisture and Ocean Salinity (SMOS) observations at L band," *Cryosphere*, vol. 14, no. 2, pp. 539–548, Feb. 2020, doi: 10.5194/tc-14-539-2020.

[36] J. Z. Miller, R. Culberg, D. G. Long, C. A. Shuman, D. M. Schroeder, and M. J. Brodzik, "An empirical algorithm to map perennial firn aquifers and ice slabs within the Greenland ice sheet using satellite L-band microwave radiometry," *Cryosphere*, vol. 16, no. 1, pp. 103–125, Jan. 2022.

[37] J. Z. Miller, D. G. Long, C. A. Shuman, R. Culberg, M. Hardman, and M. J. Brodzik, "Mapping firn saturation over Greenland using NASA's soil moisture active passive satellite," *IEEE J. Sel. Topics Appl. Earth Observ. Remote Sens.*, vol. 15, pp. 3714–3729, 2022.

[38] D. Houtz, C. Mätzler, R. Naderpour, M. Schwank, and K. Steffen, "Quantifying surface melt and liquid water on the Greenland ice sheet using L-band radiometry," *Remote Sens. Environ.*, vol. 256, Apr. 2021, Art. no. 112341, doi: 10.1016/j.rse.2021.112341.

[39] E. Bueler and J. Brown, "Shallow shelf approximation as a 'sliding law' in a thermomechanically coupled ice sheet model," *J. Geophys. Res., Earth Surf.*, vol. 114, no. F3, p. 2008, Sep. 2009, doi: 10.1029/2008jf001179.

[40] R. Winkelmann et al., "The Potsdam parallel ice sheet model (PISM-PIK)—Part 1: Model description," *Cryosphere*, vol. 5, no. 3, pp. 715–726, Sep. 2011, doi: 10.5194/tc-5-715-2011.

[41] I. M. Artemieva, "Lithosphere structure in Europe from thermal isostasy," *Earth-Sci. Rev.*, vol. 188, pp. 454–468, Jan. 2019, doi: 10.1016/j.earscirev.2018.11.004.

[42] F. Lucazeau, "Analysis and mapping of an updated terrestrial heat flow data set," *Geochemistry, Geophys., Geosyst.*, vol. 20, no. 8, pp. 4001–4024, Aug. 2019, doi: 10.1029/2019gc008389.

[43] Y. M. Martos, T. A. Jordan, M. Catalán, T. M. Jordan, J. L. Bamber, and D. G. Vaughan, "Geothermal heat flux reveals the Iceland hotspot track underneath Greenland," *Geophys. Res. Lett.*, vol. 45, no. 16, pp. 8214–8222, Aug. 2018, doi: 10.1029/2018gl078289.

[44] S. Rezvanbehbahani, L. A. Stearns, A. Kadivar, J. D. Walker, and C. J. van der Veen, "Predicting the geothermal heat flux in Greenland: A machine learning approach," *Geophys. Res. Lett.*, vol. 44, no. 24, pp. 12271–12279, Dec. 2017, doi: 10.1002/2017gl075661.

[45] W. Colgan et al., "Greenland geothermal heat flow database and map (version 1)," *Earth Syst. Sci. Data*, vol. 14, no. 5, pp. 2209–2238, May 2022, doi: 10.5194/essd-14-2209-2022.

[46] *Geothermal Heat Flux Distribution for the Greenland Ice Sheet, Derived By Combining a Global Representation and Information From Deep Ice Cores*, National Institute of Polar Research, Japan, Feb. 2019, doi: 10.20575/00000006.

[47] G. Picard, M. Sandells, and H. Löwe, "SMRT: An active–passive microwave radiative transfer model for snow with multiple microstructure and scattering formulations (v1.0)," *Geoscientific Model Develop.*, vol. 11, no. 7, pp. 2763–2788, Jul. 2018, doi: 10.5194/gmd-11-2763-2018.

[48] B. Vandecrux et al., "The SUMup collaborative database: Surface mass balance, subsurface temperature and density measurements from the Greenland and Antarctic ice sheets (2025 release)," Arctic Data Center, 2025, doi: 10.18739/A2M61BR5M.

[49] R. J. Arthern, D. G. Vaughan, A. M. Rankin, R. Mulvaney, and E. R. Thomas, "In situ measurements of Antarctic snow compaction compared with predictions of models," *J. Geophys. Res., Earth Surf.*, vol. 115, no. F3, p. 2009, Sep. 2010, doi: 10.1029/2009jf001306.

[50] C. Mätzler, *Thermal Microwave Radiation: Applications for Remote Sensing* (IET electromagnetic waves series). London, U.K.: IET, 2006, doi: 10.1049/PBEW052E.

[51] C. Yardim et al., "Greenland ice sheet subsurface temperature estimation using ultrawideband microwave radiometry," *IEEE Trans. Geosci. Remote Sens.*, vol. 60, 2022, Art. no. 4300312, doi: 10.1109/TGRS.2020.3043954.

[52] K. C. Jezek, C. Yardim, J. T. Johnson, G. Macelloni, and M. Brogioni, "Analysis of ice-sheet temperature profiles from low-frequency airborne remote sensing," *J. Glaciology*, vol. 68, no. 271, pp. 1027–1037, Mar. 2022, doi: 10.1017/jog.2022.19.

[53] Y. Duan et al., "Feasibility of estimating ice sheet internal temperatures using ultra-wideband radiometry," *IEEE Trans. Geosci. Remote Sens.*, vol. 60, 2022, Art. no. 4306611, doi: 10.1109/TGRS.2022.3208754.

[54] S. Tan et al., "A partially coherent approach for modeling polar ice sheet 0.5–2-GHz thermal emission," *IEEE Trans. Geosci. Remote Sens.*, vol. 59, no. 10, pp. 8062–8072, Oct. 2021.

[55] S. Tan et al., "Physical models of layered polar firn brightness temperatures from 0.5 to 2 GHz," *IEEE J. Sel. Topics Appl. Earth Observ. Remote Sens.*, vol. 8, no. 7, pp. 3681–3691, Jul. 2015.

[56] M. Brogioni, G. Macelloni, F. Montomoli, and K. C. Jezek, "Simulating multifrequency ground-based radiometric measurements at dome C—Antarctica," *IEEE J. Sel. Topics Appl. Earth Observ. Remote Sens.*, vol. 8, no. 9, pp. 4405–4417, Sep. 2015, doi: 10.1109/JSTARS.2015.2427512.

[57] G. D. Q. Robin, "Ice movement and temperature distribution in glaciers and ice sheets," *J. Glaciology*, vol. 2, no. 18, pp. 523–532, 1955, doi: 10.3189/002214355793702028.

[58] H. Xu, L. Tsang, J. T. Johnson, K. C. Jezek, J.-B. Yan, and P. Gogineni, "A combined active and passive method for the remote sensing of ice sheet temperature profiles," *Prog. Electromagn. Res.*, vol. 167, pp. 111–126, 2020, doi: 10.2528/pier20030601.

[59] H. Xu et al., "Polar firn properties in Greenland and Antarctica and related effects on microwave brightness temperatures," *Cryosphere*, vol. 17, no. 7, pp. 2793–2809, Jul. 2023.

[60] K. C. Jezek et al., "500–2000-MHz brightness temperature spectra of the northwestern Greenland ice sheet," *IEEE Trans. Geosci. Remote Sens.*, vol. 56, no. 3, pp. 1485–1496, Mar. 2018, doi: 10.1109/TGRS.2017.2764381.

[61] A. L. Broome, D. M. Schroeder, and J. T. Johnson, "Joint active and passive microwave thermometry of ice sheets," *IEEE Trans. Geosci. Remote Sens.*, vol. 61, 2023, Art. no. 4300310, doi: 10.1109/TGRS.2023.3255219.

[62] K. C. Jezek, M. Brogioni, J. T. Johnson, D. M. Schroeder, A. L. Broome, and G. Macelloni, "Active and passive microwave remote sensing of priestley glacier, Antarctica," *IEEE Trans. Geosci. Remote Sens.*, vol. 62, 2024, Art. no. 4302708, doi: 10.1109/TGRS.2024.3462268.

[63] A. J. Cook, A. J. Fox, D. G. Vaughan, and J. G. Ferrigno, "Retreating glacier fronts on the Antarctic peninsula over the past half-century," *Science*, vol. 308, no. 5721, pp. 541–544, Apr. 2005, doi: 10.1126/science.1104235.

[64] B. J. Davison et al., "Annual mass budget of Antarctic ice shelves from 1997 to 2021," *Sci. Adv.*, vol. 9, no. 41, p. 0186, Oct. 2023, doi: 10.1126/sciadv.adi0186.

[65] S. Wang et al., "Multidecadal pre- and post-collapse dynamics of the northern Larsen ice shelf," *Earth Planet. Sci. Lett.*, vol. 609, May 2023, Art. no. 118077, doi: 10.1016/j.epsl.2023.118077.

[66] S. Wang et al., "Controls on Larsen C ice shelf retreat from a 60-year satellite data record," *J. Geophys. Res., Earth Surf.*, vol. 127, no. 3, p. 2021, Mar. 2022, doi: 10.1029/2021jf006346.

[67] C. R. Meyer and B. M. Minchew, "Temperate ice in the shear margins of the Antarctic ice sheet: Controlling processes and preliminary locations," *Earth Planet. Sci. Lett.*, vol. 498, pp. 17–26, Sep. 2018, doi: 10.1016/j.epsl.2018.06.028.

[68] M. Brogioni et al., "Simulating 0.4–2.5 GHz brightness temperatures of the Ross ice shelf, Antarctica," *IEEE Geosci. Remote Sens. Lett.*, vol. 21, pp. 1–5, 2024, doi: 10.1109/LGRS.2024.3368613.

[69] O. Demir et al., "Measurements of 540–1740 MHz brightness temperatures of sea ice during the winter of the MOSAiC campaign," *IEEE Trans. Geosci. Remote Sens.*, vol. 60, 2022, Art. no. 5302011, doi: 10.1109/TGRS.2021.3105360.

[70] K. C. Jezek et al., "Relationships between L-band brightness temperature, backscatter, and physical properties of the Ross ice shelf Antarctica," *IEEE Trans. Geosci. Remote Sens.*, vol. 60, 2022, Art. no. 4306514, doi: 10.1109/TGRS.2022.3218538.

[71] R. Kwok, "Arctic sea ice thickness, volume, and multiyear ice coverage: Losses and coupled variability (1958–2018)," *Environ. Res. Lett.*, vol. 13, no. 10, Oct. 2018, Art. no. 105005, doi: 10.1088/1748-9326/aae3ec.

[72] J. C. Comiso, W. N. Meier, and R. Gersten, "Variability and trends in the Arctic sea ice cover: Results from different techniques," *J. Geophys. Res., Oceans*, vol. 122, no. 8, pp. 6883–6900, Aug. 2017, doi: 10.1002/2017jc012768.

[73] J. C. Comiso, "Warming trends in the Arctic from clear sky satellite observations," *J. Climate*, vol. 16, no. 21, pp. 3498–3510, Nov. 2003, doi: 10.1175/1520-0442(2003)016<3498:wtitaf>2.0.co;2.

[74] M. A. Tschudi, W. N. Meier, and J. S. Stewart, "An enhancement to sea ice motion and age products at the national snow and ice data center (NSIDC)," *Cryosphere*, vol. 14, no. 5, pp. 1519–1536, May 2020, doi: 10.5194/tc-14-1519-2020.

[75] Core Writing Team, H. Lee and J. Romero, Eds., "Climate change 2023: Synthesis report. Contribution of working groups I, II and III to the sixth assessment report of the intergovernmental panel on climate change [core writing team]," IPCC, Geneva, Switzerland, pp. 35–115, 2023, doi: 10.59327/IPCC/AR6-9789291691647.

[76] B. J. Peterson, J. McClelland, R. Curry, R. M. Holmes, J. E. Walsh, and K. Aagaard,

"Trajectory shifts in the Arctic and subarctic freshwater cycle," *Science*, vol. 313, no. 5790, pp. 1061–1066, Aug. 2006, doi: 10.1126/science.1122593.

[77] F. A. Haumann, N. Gruber, and M. Münnich, "Sea-ice induced southern ocean subsurface warming and surface cooling in a warming climate," *AGU Adv.*, vol. 1, no. 2, p. 2019, Jun. 2020, doi: 10.1029/2019av000132.

[78] Q. Wang et al., "Intensification of the Atlantic water supply to the Arctic ocean through fram strait induced by Arctic sea ice decline," *Geophys. Res. Lett.*, vol. 47, no. 3, p. 2019, Feb. 2020, doi: 10.1029/2019gl086682.

[79] S. Lind, R. B. Ingvaldsen, and T. Furevik, "Arctic warming hotspot in the northern Barents sea linked to declining sea-ice import," *Nature Climate Change*, vol. 8, no. 7, pp. 634–639, Jul. 2018, doi: 10.1038/s41558-018-0205-y.

[80] F. Sévellec, A. V. Fedorov, and W. Liu, "Arctic sea-ice decline weakens the Atlantic meridional overturning circulation," *Nature Climate Change*, vol. 7, no. 8, pp. 604–610, Aug. 2017, doi: 10.1038/nclimate3353.

[81] Ø. Skagseth, T. Eldevik, M. Årthun, H. Asbjørnsen, V. S. Lien, and L. H. Smedsrud, "Reduced efficiency of the Barents sea cooling machine," *Nature Climate Change*, vol. 10, no. 7, pp. 661–666, Jul. 2020, doi: 10.1038/s41558-020-0772-6.

[82] M. Vancoppenolle, T. Fichefet, H. Goosse, S. Bouillon, G. Madec, and M. A. M. Maqueda, "Simulating the mass balance and salinity of Arctic and Antarctic sea ice. 1. model description and validation," *Ocean Model.*, vol. 27, nos. 1–2, pp. 33–53, Jan. 2009, doi: 10.1016/j.ocemod.2008.10.005.

[83] P. Gloersen, W. J. Campbell, D. J. Cavalieri, J. C. Comiso, C. L. Parkinson, and H. J. Zwally, "Satellite passive microwave observations and analysis of Arctic and Antarctic sea ice, 1978–1987," *Ann. Glaciology*, vol. 17, pp. 149–154, Jan. 1993, doi: 10.3189/s0260305500012751.

[84] T. Lavergne, S. Eastwood, Z. Teffah, H. Schyberg, and L. A. Breivik, "Sea ice motion from low-resolution satellite sensors: An alternative method and its validation in the Arctic," *J. Geophys. Res.*, vol. 115, no. C10, p. 2009, Oct. 2010, doi: 10.1029/2009jc005958.

[85] R. Ricker, S. Hendricks, V. Helm, H. Skourup, and M. Davidson, "Sensitivity of CryoSat-2 Arctic sea-ice freeboard and thickness on radar-waveform interpretation," *Cryosphere*, vol. 8, no. 4, pp. 1607–1622, Aug. 2014, doi: 10.5194/tc-8-1607-2014.

[86] X. Tian-Kunze et al., "SMOS-derived thin sea ice thickness: Algorithm baseline, product specifications and initial verification," *Cryosphere*, vol. 8, no. 3, pp. 997–1018, May 2014, doi: 10.5194/tc-8-997-2014.

[87] L. Kaleschke et al., "SMOS sea ice product: Operational application and validation in the Barents sea marginal ice zone," *Remote Sens. Environ.*, vol. 180, pp. 264–273, Jul. 2016, doi: 10.1016/j.rse.2016.03.009.

[88] T. Lavergne et al., "A new structure for the sea ice essential climate variables of the global climate observing system," *Bull. Amer. Meteorological Soc.*, vol. 103, no. 6, pp. E1502–E1521, Jun. 2022, doi: 10.1175/bams-d-21-0227.1.

[89] M. Tiuri, M. Hallikainen, and A. Lääperi, "Radiometer studies of low-salinity sea ice," *Boundary-Layer Meteorol.*, vol. 13, nos. 1–4, pp. 361–371, Jan. 1978, doi: 10.1007/bf00913882.

[90] M. T. Hallikainen, "A new low-salinity sea-ice model for UHF radiometry," *Int. J. Remote Sens.*, vol. 4, no. 3, pp. 655–681, Jan. 1983, doi: 10.1080/01431168308948581.

[91] J. D. Menashi, K. M. St. Germain, C. T. Swift, J. C. Comiso, and A. W. Lohanick, "Low-frequency passive-microwave observations of sea ice in the Weddell sea," *J. Geophys. Res., Oceans*, vol. 98, no. 12, pp. 22569–22577, Dec. 1993, doi: 10.1029/93jc02058.

[92] M. J. Mei, T. Maksym, B. Weissling, and H. Singh, "Estimating early-winter Antarctic sea ice thickness from deformed ice morphology," *Cryosphere*, vol. 13, no. 11, pp. 2915–2934, Nov. 2019, doi: 10.5194/tc-13-2915-2019.

[93] J. C. Landy, A. A. Petty, M. Tsamados, and J. C. Stroeve, "Sea ice roughness overlooked as a key source of uncertainty in CryoSat-2 ice freeboard retrievals," *J. Geophys. Res., Oceans*, vol. 125, no. 5, p. 2019, May 2020, doi: 10.1029/2019jc015820.

[94] A. A. Petty, N. T. Kurtz, R. Kwok, T. Markus, and T. A. Neumann, "Winter Arctic sea ice thickness from ICESat-2 freeboards," *J. Geophys. Res., Oceans*, vol. 125, no. 5, p. 2019, May 2020, doi: 10.1029/2019jc015764.

[95] S. Kacimi and R. Kwok, "The Antarctic sea ice cover from ICESat-2 and CryoSat-2: Freeboard, snow depth, and ice thickness," *Cryosphere*, vol. 14, no. 12, pp. 4453–4474, Dec. 2020, doi: 10.5194/tc-14-4453-2020.

[96] L. Kaleschke, X. Tian-Kunze, S. Hendricks, and R. Ricker, "SMOS-derived Antarctic thin sea ice thickness: Data description and validation in the Weddell sea," *Earth Syst. Sci. Data*, vol. 16, no. 7, pp. 3149–3170, Jul. 2024.

[97] K. C. Jezek et al., "Remote sensing of sea ice thickness and salinity with 0.5–2 GHz microwave radiometry," *IEEE Trans. Geosci. Remote Sens.*, vol. 57, no. 11, pp. 8672–8684, Nov. 2019, doi: 10.1109/TGRS.2019.2922163.

[98] O. Demir et al., "Studies of sea-ice thickness and salinity retrieval using 0.5–2 GHz microwave radiometry," *IEEE Trans. Geosci. Remote Sens.*, vol. 60, 2022, Art. no. 4304412, doi: 10.1109/TGRS.2022.3168646.

[99] F. Hernández-Macià, C. Gabarró, M. Huntemann, R. Naderpour, J. T. Johnson, and K. C. Jezek, "On sea ice emission modeling for MOSAiC's L-band radiometric measurements," *Ann. Glaciology*, vol. 65, pp. 1–14, Oct. 2024, doi: 10.1017/aog.2024.38.

[100] M. R. Vant, R. O. Ramseier, and V. Makios, "The complex-dielectric constant of sea ice at frequencies in the range 0.1–40 GHz," *J. Appl. Phys.*, vol. 49, no. 3, pp. 1264–1280, Mar. 1978, doi: 10.1063/1.325018.

[101] M. Brogioni et al., "Ice sheet and sea ice ultrawideband microwave radiometric airborne eXperiment (ISSIUMAX) in Antarctica: First results from Terra Nova bay," *Cryosphere*, vol. 17, no. 1, pp. 255–278, Jan. 2023, doi: 10.5194/tc-17-255-2023.

[102] M. Brogioni et al., "500–2000-MHz airborne brightness temperature measurements over the east Antarctic Plateau," *IEEE Geosci. Remote Sens. Lett.*, vol. 19, pp. 1–5, 2022, doi: 10.1109/LGRS.2021.3056740.

[103] M. Hoppmann et al., "Platelet ice, the southern ocean's hidden ice: A review," *Ann. Glaciology*, vol. 61, no. 83, pp. 341–368, Dec. 2020.

[104] P. J. Langhorne et al., "Fast ice thickness distribution in the western Ross sea in late spring," *J. Geophys. Res., Oceans*, vol. 128, no. 2, Feb. 2023, Art. no. e2022JC019459, doi: 10.1029/2022JC019459.

[105] W. Rack, D. Price, C. Haas, P. J. Langhorne, and G. H. Leonard, "Sea ice thickness in the western Ross sea," *Geophys. Res. Lett.*, vol. 48, no. 1, Jan. 2021, Art. no. e2020GL090866, doi: 10.1029/2020GL090866.

[106] L. Kaleschke et al., "Earth explorer 12 candidate mission CryoRad: Innovations in sea ice observations," presented at the ESA Living Planet Symp., Jun. 2025.

[107] Intergovernmental Oceanographic Commission of the United Nations Educational. *The 2022 GCOS ECVs Requirements (GCOS 245)*. Accessed: Jan. 21, 2025. [Online]. Available: https://library.wmo.int/records/item/58111-the-2022-gcos-ecvs-requirements-gcos-245

[108] E. C. Carmack, "The alpha/beta ocean distinction: A perspective on freshwater fluxes, convection, nutrients and productivity in high-latitude seas," *Deep Sea Res. II, Topical Stud. Oceanogr.*, vol. 54, nos. 23–26, pp. 2578–2598, Nov. 2007, doi: 10.1016/j.dsr2.2007.08.018.

[109] M.-L. Timmermans and J. Marshall, "Understanding Arctic ocean circulation: A review of ocean dynamics in a changing climate," *J. Geophys. Res., Oceans*, vol. 125, no. 4, p. 2018, Apr. 2020, doi: 10.1029/2018jc014378.

[110] M. P. Meredith, "The global importance of the southern ocean and the key role of its freshwater cycle," *Ocean Challenge*, vol. 23, no. 2, pp. 27–32, 2019.

[111] N. C. Swart et al., "The southern ocean freshwater input from Antarctica (SOFIA) initiative: Scientific objectives and experimental design," *Geoscientific Model Develop.*, vol. 16, no. 24, pp. 7289–7309, Dec. 2023, doi: 10.5194/gmd-16-7289-2023.

[112] W. Liu, S.-P. Xie, Z. Liu, and J. Zhu, "Overlooked possibility of a collapsed Atlantic meridional overturning circulation in warming climate," *Sci. Adv.*, vol. 3, no. 1, Jan. 2017, Art. no. 1601666, doi: 10.1126/sciadv.1601666.

[113] P. Ditlevsen and S. Ditlevsen, "Warning of a forthcoming collapse of the Atlantic meridional overturning circulation," *Nature Commun.*, vol. 14, no. 1, p. 4254, Jul. 2023, doi: 10.1038/s41467-023-39810-w.

[114] A. Purich and E. W. Doddridge, "Record low Antarctic sea ice coverage indicates a new sea ice state," *Commun. Earth Environ.*, vol. 4, no. 1, p. 314, Sep. 2023, doi: 10.1038/s43247-023-00961-9.

[115] S. A. Grodsky, N. Reul, and D. Vandemark, "Sea surface salinity response to variations in the aleutian low," *J. Mar. Syst.*, vol. 240, May 2023, Art. no. 103888, doi: 10.1016/j.jmarsys.2023.103888.

[116] G. Reverdin, F. Bonjean, L. Kilian, J. Boutin, S. Guimbard, J. L. Vergely, N. Foukal, Femke de Jong, C. Stedmon, and D. Khvorostyanov, "Sea surface salinity variability from satellite and in situ observations around Greenland," *JAOTech*, 2025, doi: 10.1175/JTECH-D-24-0105.1.

[117] P. A. Hudson, A. C. H. Martin, S. A. Josey, A. Marzocchi, and A. Angeloudis, "Drivers of laptev sea interannual variability in salinity and temperature," *Ocean Sci.*, vol. 20, no. 2, pp. 341–367, Mar. 2024, doi: 10.5194/os-20-341-2024.

[118] S. Tajouri et al., "Simulated impact of time-varying river runoff and Greenland freshwater discharge on sea level variability in the Beaufort gyre over 2005–2018," *JGR Oceans*, vol. 129, no. 9, p. 2024, Sep. 2024, doi: 10.1029/2024jc021237.

[119] S. B. Hall, B. Subrahmanyam, and M. Steele, "The role of the Russian shelf in seasonal and interannual variability of Arctic sea surface salinity and freshwater content," *J. Geophys. Res., Oceans*, vol. 128, no. 1, p. 2022, Jan. 2023, doi: 10.1029/2022jc019247.

[120] L. Crews, C. M. Lee, L. Rainville, and J. Thomson, "Direct observations of the role of lateral advection of sea ice meltwater in the onset of autumn freeze up," *J. Geophys. Res., Oceans*, vol. 127, no. 2, p. 2021, Feb. 2022, doi: 10.1029/2021jc017775.

[121] C. Van Straaten, C. Lique, and N. Kolodziejcyk, "The life cycle of the low salinity lenses at the surface of the Arctic ocean," *J. Geophys. Res., Oceans*, vol. 130, no. 4, p. 2024, Apr. 2025, doi: 10.1029/2024jc021699.

[122] H. Zhang, X. Bai, and K. Wang, "Response of the Arctic sea ice–ocean system to meltwater perturbations based on a one-dimensional model study," *Ocean Sci.*, vol. 19, no. 6, pp. 1649–1668, Nov. 2023, doi: 10.5194/os-19-1649-2023.

[123] D. M. Le Vine and E. P. Dinnat, "Sensitivity of wide bandwidth radiometer for remote sensing of ocean salinity," *IEEE Trans. Geosci. Remote Sens.*, vol. 60, 2022, Art. no. 5301517, doi: 10.1109/TGRS.2021.3101962.

[124] D. M. Le Vine and E. P. Dinnat, "Measurement of SST and SSS using frequencies in the range 0.3–2.0 GHz," *Radio Sci.*, vol. 57, no. 4, p. 2021, Apr. 2022, doi: 10.1029/2021rs007415.

[125] D. M. Le Vine, R. H. Lang, M. Li, E. P. Dinnat, J. Boutin, and Y. Zhou, "The dielectric constant of sea water at P-band for salinity from 0 to 150 pss," *IEEE Trans. Geosci. Remote Sens.*, vol. 63, 2025, Art. no. 4202011, doi:

10.1109/TGRS.2025.3532180.
[126] M. D. Anguelova et al., "FOAM emissivity modelling with foam properties tuned by frequency and polarization," in *Proc. IEEE Int. Geosci. Remote Sens. Symp.*, Jul. 2022, pp. 6923–6926, doi: 10.1109/IGARSS46834.2022.9883610.
[127] J. Boutin et al., "New seawater dielectric constant parametrization and application to SMOS retrieved salinity," *IEEE Trans. Geosci. Remote Sens.*, vol. 61, 2023, Art. no. 2000813, doi: 10.1109/TGRS.2023.3257923.
[128] J. Blyverket, P. D. Hamer, P. Schneider, C. Albergel, and W. A. Lahoz, "Monitoring soil moisture drought over northern high latitudes from space," *Remote Sens.*, vol. 11, no. 10, p. 1200, May 2019, doi: 10.3390/rs11101200.
[129] Y. H. Kerr et al., "Overview of SMOS performance in terms of global soil moisture monitoring after six years in operation," *Remote Sens. Environ.*, vol. 180, pp. 40–63, Jul. 2016, doi: 10.1016/j.rse.2016.02.042.
[130] M. S. Burgin et al., "A comparative study of the SMAP passive soil moisture product with existing satellite-based soil moisture products," *IEEE Trans. Geosci. Remote Sens.*, vol. 55, no. 5, pp. 2959–2971, May 2017, doi: 10.1109/TGRS.2017.2656859.
[131] M. J. Escorihuela, A. Chanzy, J. P. Wigneron, and Y. H. Kerr, "Effective soil moisture sampling depth of L-band radiometry: A case study," *Remote Sens. Environ.*, vol. 114, no. 5, pp. 995–1001, May 2010, doi: 10.1016/j.rse.2009.12.011.
[132] B. J. Choudhury, T. J. Schmugge, and T. Mo, "A parameterization of effective soil temperature for microwave emission," *J. Geophys. Res., Oceans*, vol. 87, no. 2, pp. 1301–1304, Feb. 1982, doi: 10.1029/jc087ic02p01301.
[133] T. J. Jackson, T. J. Schmugge, and J. R. Wang, "Passive microwave sensing of soil moisture under vegetation canopies," *Water Resour. Res.*, vol. 18, no. 4, pp. 1137–1142, Aug. 1982, doi: 10.1029/wr018i004p01137.
[134] M. Brandt et al., "Satellite passive microwaves reveal recent climate-induced carbon losses in African drylands," *Nature Ecol. Evol.*, vol. 2, no. 5, pp. 827–835, Apr. 2018, doi: 10.1038/s41559-018-0530-6.
[135] N. J. Rodríguez-Fernández et al., "An evaluation of SMOS L-band vegetation optical depth (L-VOD) data sets: High sensitivity of L-VOD to above-ground biomass in Africa," *Biogeosciences*, vol. 15, no. 14, pp. 4627–4645, Jul. 2018, doi: 10.5194/bg-15-4627-2018.
[136] R. Rahmoune, P. Ferrazzoli, Y. K. Singh, Y. H. Kerr, P. Richaume, and A. Al Bitar, "SMOS retrieval results over forests: Comparisons with independent measurements," *IEEE J. Sel. Topics Appl. Earth Observ. Remote Sens.*, vol. 7, no. 9, pp. 3858–3866, Sep. 2014, doi: 10.1109/JSTARS.2014.2321027.
[137] J.-P. Wigneron et al., "Tropical forests did not recover from the strong 2015–2016 el Niño event," *Sci. Adv.*, vol. 6, no. 6, p. 4603, Feb. 2020, doi: 10.1126/sciadv.aay4603.
[138] Y. Dou et al., "Reliability of using vegetation optical depth for estimating decadal and interannual carbon dynamics," *Remote Sens. Environ.*, vol. 285, Feb. 2023, Art. no. 113390, doi: 10.1016/j.rse.2022.113390.
[139] L. Fan et al., "Satellite-observed pantropical carbon dynamics," *Nature Plants*, vol. 5, no. 9, pp. 944–951, Jul. 2019, doi: 10.1038/s41477-019-0478-9.
[140] R. H. Waring and J. F. Franklin, "Evergreen coniferous forests of the Pacific northwest: Massive long-lived conifers dominating these forests are adapted to a winter-wet, summer-dry environment," *Science*, vol. 204, no. 4400, pp. 1380–1386, Jun. 1979, doi: 10.1126/science.204.4400.1380.
[141] J. C. Salazar-Neira et al., "Above-ground biomass estimation based on multi-angular L-band measurements of brightness temperatures," *IEEE J. Sel. Topics Appl. Earth Observ. Remote Sens.*, vol. 16, pp. 5813–5827, 2023, doi: 10.1109/JSTARS.2023.3285288.
[142] X. Shen et al., "Soil moisture retrieval depth of P- and L-band radiometry: Predictions and observations," *IEEE Trans. Geosci. Remote Sens.*, vol. 59, no. 8, pp. 6814–6822, Aug. 2021, doi: 10.1109/TGRS.2020.3026384.
[143] X. Shen et al., "Impact of random and periodic surface roughness on P- and L-band radiometry," *Remote Sens. Environ.*, vol. 269, Feb. 2022, Art. no. 112825, doi: 10.1016/j.rse.2021.112825.
[144] X. Huang, Z. H. Shi, H. D. Zhu, H. Y. Zhang, L. Ai, and W. Yin, "Soil moisture dynamics within soil profiles and associated environmental controls," *CATENA*, vol. 136, pp. 189–196, Jan. 2016, doi: 10.1016/j.catena.2015.01.014.
[145] A. Tabatabaeenejad, M. Burgin, X. Duan, and M. Moghaddam, "P-band radar retrieval of subsurface soil moisture profile as a second-order polynomial: First AirMOSS results," *IEEE Trans. Geosci. Remote Sens.*, vol. 53, no. 2, pp. 645–658, Feb. 2015, doi: 10.1109/TGRS.2014.2326839.
[146] F. Brakhasi et al., "Soil moisture profile estimation under bare and vegetated soils using combined L-band and P-band radiometer observations: An incoherent modeling approach," *Remote Sens. Environ.*, vol. 307, Jun. 2024, Art. no. 114148, doi: 10.1016/j.rse.2024.114148.
[147] F. Brakhasi et al., "Towards soil moisture profile estimation in the root zone using L- and P-band radiometer observations: A coherent modelling approach," *Sci. Remote Sens.*, vol. 7, Jun. 2023, Art. no. 100079, doi: 10.1016/j.srs.2023.100079.
[148] Y. Zhou et al., "Microwave emission model for layered vegetation (MEMLV): An exemplary study for coniferous forests from P- to Ka-band," *IEEE Trans. Geosci. Remote Sens.*, vol. 62, 2024, Art. no. 4417220, doi: 10.1109/TGRS.2024.3491218.
[149] F. Brakhasi et al., "A comparison of passive microwave emission models for estimating brightness temperature at L- and P-bands under bare and vegetated soil conditions," *IEEE J. Sel. Topics Appl. Earth Observ. Remote Sens.*, vol. 17, pp. 2570–2585, 2024, doi: 10.1109/JSTARS.2023.3344764.
[150] M. Schwank, R. Naderpour, and C. Mätzler, "'Tau-Omega'- and two-stream emission models used for passive L-band retrievals: Application to close-range measurements over a forest," *Remote Sens.*, vol. 10, no. 12, p. 1868, Nov. 2018, doi: 10.3390/rs10121868.
[151] X. Shen et al., "Evaluation of the tau-omega model over bare and wheat-covered flat and periodic soil surfaces at P- and L-band," *Remote Sens. Environ.*, vol. 273, May 2022, Art. no. 112960, doi: 10.1016/j.rse.2022.112960.
[152] X. Shen et al., "Evaluation of the tau-omega model over a dense corn canopy at P- and L-band," *IEEE Geosci. Remote Sens. Lett.*, vol. 20, pp. 1–5, 2023, doi: 10.1109/LGRS.2023.3315869.
[153] X. Shen et al., "P-band radiometry for enhanced vegetation optical depth (VOD) and soil moisture retrieval in dense crop canopies," *Remote Sens. Environ.*, vol. 313, Nov. 2024, Art. no. 114353, doi: 10.1016/j.rse.2024.114353.
[154] G. Macelloni et al., "Cryorad: A low frequency wideband radiometer mission for the study of the cryosphere," in *Proc. IEEE Int. Geosci. Remote Sens. Symp.*, Jul. 2018, pp. 1998–2000.
[155] M. J. Andrews et al., "The ultrawideband software-defined microwave radiometer: Instrument description and initial campaign results," *IEEE Trans. Geosci. Remote Sens.*, vol. 56, no. 10, pp. 5923–5935, Oct. 2018, doi: 10.1109/TGRS.2018.2828604.
[156] G. Macelloni et al., "Preliminary study for a spaceborne ultrawideband microwave radiometer for the monitoring of cryosphere elements: The cryorad project," in *Proc. IEEE Int. Geosci. Remote Sens. Symp. (IGARSS)*, Jul. 2017, pp. 1185–1188, doi: 10.1109/IGARSS.2017.8127169.
[157] J. Johnson, K. C. Jezek, and G. Macelloni, "Monitoring Earth's ice sheets, sea ice, and polar seas with 0.5–2 GHz microwave radiometry: The PolarRad mission," presented at the IGARSS, 2023.

## ABOUT THE AUTHORS

**Giovanni Macelloni** (Senior Member, IEEE) received the M.Sc. degree in electronic engineering from the University of Florence, Florence, Italy, in 1993.

He is currently the Director of the Institute of Applied Physics "Nello Carrara"—National Research Country, Sesto Fiorentino, Italy, and an Adjunct Professor with the University of Venice. He is also the Science Lead of the ESA's EE12 Candidate Mission CryoRad. He is the National Delegate of SCAR and Global Cryosphere Watch of the WMO. He has worked as a tutor for Ph.D. students. His research has been carried out in the framework of several national and international programs granted by Italian entities, European Community, and Space agencies (ESA, ASI, NASA, and JAXA), and includes participation in international teams for the study of the cryosphere and the development and assessment of future spaceborne missions. His research interests include microwave active and passive remote sensing for the study of the Earth system and the cryosphere in particular. He is also involved in the design and development of microwave remote sensing systems, both from the ground, the air, and satellites.

Mr. Macelloni served as a reviewer for several international committees, organizations, and international journals, and acted as an organizer and the co-chair of international conferences. He is an Associate Editor of IEEE TRANSACTIONS ON GEOSCIENCE AND REMOTE SENSING.

**Kenneth C. Jezek** received the B.S. degree in physics from the University of Illinois Urbana–Champaign, Urbana, IL, USA, in 1973, and the M.Sc. and Ph.D. degrees in geophysics from the University of Wisconsin–Madison, Madison, WI, USA, in 1997 and 1980, respectively.

He was a Geophysicist with the U.S. Army Cold Regions Research and Engineering Laboratory, Hanover, NH, USA. He joined the Byrd Polar and Climate Research Center, The Ohio State University (OSU), Columbus, OH, USA, as the Director, in 1989, where is a Professor Emeritus with the School of Earth Sciences. His most recent interests include the application of ultra-wideband radiometry to ice sheet and sea ice studies.

**Marco Brogioni** (Member, IEEE) was born in Siena, Italy, in 1976. He received the M.Sc. degree in telecommunications engineering from the University of Siena, Siena, in 2003, and the Ph.D. degree in remote sensing from the University of Pisa, Pisa, Italy, in 2008.

Since 2004, he has been with the Microwave Remote Sensing Group, Institute of Applied Physics "Nello Carrara" (IFAC), National Research Council of Italy (CNR), Florence, Italy. From 2006 to 2007, he was a Visiting Student with the University of California, Santa Barbara, Santa Barbara, CA, USA, working on the microwave modeling of snow-covered surfaces. Most of his activities are carried out in the framework of ESA and ASI projects. He is also involved in the design and manufacturing of microwave radiometers (P–Ka bands). Since 2021, he has been leading the development of the CryoRad ultra-wideband airborne demonstrator in the framework of Italian Space Agency Project. He is currently involved in several international projects regarding polar regions. He is part of the ESA Soil Moisture and Ocean Salinity (SMOS) L1 Team and a former but still active with the NASA ESTO UWBRAD Team. His research interests include passive and active microwave remote sensing applied to snow by using satellite- and ground-based data, especially the development of electromagnetic models for passive and active microwave remote sensing of snow, vegetation, and soil.

Dr. Brogioni was a recipient of the Third Prize at the URSI GA Student Prize Paper Competition, Chicago, IL, USA, in 2008. He served as the Co-Chair for the 16th MicroRad 2020 IEEE Meeting, the Local Organizing Committee of the 10th Microrad, Florence, in 2008, and the Microwave Signature Symposium of the URSI Commission-F, Florence, in 2010. He participated in Italian Antarctic Expeditions as a PI and a Field Campaign Leader, carrying out his research at Concordia Station (Dome-C) and Mario Zucchelli Station (Ross Sea) in 2013, 2015, and 2018. He is currently a PI of the ESA Earth Explorer 12 CryoRad Phase 0 scientific study.

**Joel T. Johnson** (Fellow, IEEE) received the Bachelor of Electrical Engineering degree from Georgia Institute of Technology, Atlanta, GA, USA, in 1991, and the S.M. and Ph.D. degrees from Massachusetts Institute of Technology, Cambridge, MA, USA, in 1993 and 1996, respectively.

He is currently the Burn and Sue Lin Professor with the Department of Electrical and Computer Engineering and the ElectroScience Laboratory, The Ohio State University, Columbus, OH, USA. His research interests are in the areas of microwave remote sensing, propagation, and electromagnetic wave theory.

Dr. Johnson is a member of Commissions B and F of the International Union of Radio Science (URSI), Tau Beta Pi, Eta Kappa Nu, and Phi Kappa Phi. He received the 1993 Best Paper Award from the IEEE Geoscience and Remote Sensing Society, was named an Office of Naval Research Young Investigator and National Science Foundation Career awardee, was a recipient of the PECASE Award in 1997, and was recognized by the U.S. National Committee of URSI as a Booker Fellow in 2002. He currently serves as the Deputy Editor-in-Chief for IEEE TRANSACTIONS ON GEOSCIENCE AND REMOTE SENSING.

**Marion Leduc-Leballeur** received the M.Sc. degree in remote sensing and the Ph.D. degree in atmospheric physics from the University Pierre and Marie Curie (UPMC), Paris, France, in 2008 and 2012, respectively.

Her work was conducted at the Laboratoire Atmosphères, Milieux, Observations Spatiales (LATMOS), Institut Pierre-Simon Laplace (IPSL), UPMC. From 2012 to 2016, she was a Research Engineer with the Institute of Environmental Geosciences (IGE), Grenoble, France, to take part in remote sensing activities in Antarctica with the support of a postdoctoral grant of two years from French Space Agency (CNES) about using Soil Moisture and Ocean Salinity (SMOS) observations to investigate snow properties of the Antarctic ice sheet. In 2017, she joined IFAC-CNR, Sesto Fiorentino, Italy, as a Scientist, working with the Microwave Remote Sensing Group to focus on the study of snow/ice properties from in situ measurements, satellite observations, reanalyses, and models data, and electromagnetic models. Her field of research is the study of the cryosphere through passive microwave satellite observations.

**Ghislain Picard** received the M.Sc. degree in remote sensing from the University of Paris VII, Paris, France, in 1997, and the Ph.D. degree from the Center d'Etudes Spatiale de la Biosphere (CESBIO), Toulouse, France, in 2002.

In 2005, he joined the Institut des Géosciences de l'Environnement, Université Grenoble-Alpes, Grenoble, France, where since 2018, he has been a Full Professor. He is involved in the development of innovative instruments for the characterization of the snow-physical properties and of optical and microwave radiative transfer (RT) models. His research interests include the antarctic climate observed through the study of snow using a variety of remote sensing techniques and field experimentation.

**Ange Haddjeri** received the M.Sc. degree in oceanic, atmospheric, and climate science from Claude Bernard University Lyon 1, Villeurbanne, France, in 2020, and the Ph.D. degree in alpine snowpack variability modeling from Paul Sabatier University, Toulouse, France, in 2024.

His research interests include Alpine blowing snow variability, snow and ice modeling, and the application of visible and microwave remote sensing.

**Lars Kaleschke** received the M.Sc. and Ph.D. degrees in physics from the University of Bremen, Bremen, Germany, in 1998 and 2003, respectively.

From 2006 to 2018, he was a Professor with the Institute of Oceanography, Universität Hamburg, Hamburg, Germany, where he contributed to the DFG Cluster of Excellence for climate research. In 2019, he joined the Alfred Wegener Institute, Bremerhaven, Germany, and took part in the longest leg of the MOSAiC expedition. His measurements of sea ice using microwave radiometers provide a basis for the development, validation, and future improvement of satellite-based methods for observing the polar regions. He is currently a Senior Scientist with the Sea Ice Physics Section at the Alfred Wegener Institute and serves on the ESA CryoRad Mission Advisory Group.

**Jacqueline Boutin** (Member, IEEE) received the Ph.D. degree in physical methods in remote sensing from the University of Paris VII, Paris, France, in 1990.

She is a Senior Research Scientist with the Centre National de la Recherche Scientifique (CNRS) and the Deputy Director of the Laboratoire d'Océanographie et du Climat-Expérimentations et Approches Numériques (LOCEAN), Paris. She has widely studied the validity of remotely sensed wind speeds and the ocean–atmosphere exchange of $CO_2$ at a large scale using both satellite (wind speeds, sea surface temperature, and ocean color) and in situ data (in particular, carbon-interface ocean–atmosphere autonomous drifters, CARIOCA). Since 1999, she has been involved in the Soil Moisture and Ocean Salinity (SMOS) mission. She participated in the development of an L-band sea surface emissivity model and in several airborne campaigns (WISE and EuroSTARRS). She coordinates the scientific activities of French SMOS-Ocean Team, European Space Agency (ESA) Climate Change Initiative Sea Surface Salinity Project, and she participates with the ESA Expert Support Laboratories that define and validate the processing of SMOS Level 2 measurements for the retrieval of sea surface salinity.

**Jean Luc Vergely** received the Engineering degree from the Ecole Nationale du Génie des Eaux et de l'Environnement de Strasbourg, Strasbourg, France, in 1988, and the Ph.D. degree in statistics applied to astronomy from Louis Pasteur University, Strasbourg, in 1998.

He is currently with ACRI-ST, Sophia Antipolis, France. Since 2003, he has been involved in the Soil Moisture and Ocean Salinity (SMOS) mission, where he contributes to the development of levels 2–4 data processing, particularly regarding the characterization of random and systematic uncertainties. Specializing in inverse methods, he also works on the implementation of tomographic techniques applied both to the Earth's atmosphere and to the interstellar medium.

**Nicolas Kolodziejczyk** received the Ph.D. degree from the University of Brest, in 2008.

From 2012 to 2015, he started to work with L-band satellite measurements during his postdoctoral research at Sorbonne University. In 2015, he joined the University of Brest, as a Professor of physical oceanography with responsibilities on the Service National d'Observation Argo France, SNO/INSU/OSU IUEM, Plouzané, France. His research interests include the observation of ocean circulation and water masses interannual variability; ocean salinity and its role in ocean dynamics from low to high latitudes; data analysis methods and products; and ocean dissolved oxygen variability.

**Laurent Bertino** was born in Saint-Jean-de-Maurienne, France, in 1975. He received the Ph.D. degree in geostatistics from the École des Mines de Paris, Paris, France, in 2001.

He has specialized in numerical ocean and sea ice modeling using ensemble-based data assimilation techniques. He has been working with the Nansen Center, since 2002, setting up the TOPAZ system using the HYCOM ocean model and the ensemble Kalman filter. He is currently leading the Data Assimilation Group, Nansen Center, and the Arctic Monitoring.

**Emmanuel P. Dinnat** (Senior Member, IEEE) received the Advanced Studies degree in instrumental methods in astrophysics and spatial applications and the Ph.D. degree in computer science, telecommunications, and electronics from the Pierre and Marie Curie University, Paris, France, in 1999 and 2003, respectively.

He is a Research Scientist with the Cryospheric Sciences Laboratory, NASA Goddard Space Flight Center (GSFC), Greenbelt, MD, USA. He has been working on the calibration, retrieval algorithm development, and science product validation for various airborne experiments and satellite missions. His research interests include active and passive microwave remote sensing, sea surface salinity, scattering from rough surfaces, atmospheric radiative transfer, and numerical simulations. His latest research focuses on high-latitude oceanography and the interactions between the cryosphere and oceans.

**Rasmus T. Tonboe** received the M.Sc. degree in geology from the University of Aarhus, Aarhus, Denmark, in 1997, and the Ph.D. degree in geophysics from the University of Copenhagen, Copenhagen, Denmark, in 2004.

From 1997 to 2021, he worked as a Research Scientist with the Danish Meteorological Institute. He is currently an Associate Professor with the Technical University of Denmark, Copenhagen. He is engaged in the development of new climate data records using historical satellite data from the 1970s until today. He has field work experience, operating radiometers in the field, snow, and sea ice sampling, and installing meteorological monitoring stations on sea ice. His research interests also include microwave and infrared remote sensing of sea ice, in particular, modeling of thermal emission and backscatter from sea ice and the use of forward model inversion for estimating sea ice snow cover, and other properties.

**Anne Munck Solgaard** is a Senior Researcher with the Geological Survey of Denmark and Greenland (GEUS), Copenhagen, Denmark. She has a strong expertise in combining numerical models, EO data, and in situ observations to study the dynamics and processes of ice. In her current position, she is in charge of the PROMICE ice velocity product for Greenland from Sentinel-1 SAR data and has contributed significantly to the development of other operational products estimating the components of mass loss from the Greenland ice sheet. She has a background in numerical ice flow modeling, applying models to explore the initiation and evolution of the Greenland ice sheet as well as seasonal scale changes in basal conditions at smaller scales. Her main field of research is within ice sheet dynamics and how it relates to climate forcing on long and short timescales.

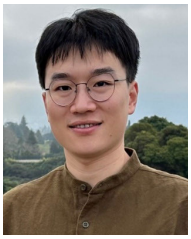

**Xiaoji Shen** (Member, IEEE) received the Ph.D. degree in civil engineering from Monash University, Clayton, VIC, Australia, in 2022.

He is currently a Research Professor with the College of Surveying and Geo-Informatics, Tongji University, Shanghai, China. His research interests include subsurface soil moisture retrieval and electromagnetic modeling of P-band radiometry.

**Jeffrey P. Walker** (Fellow, IEEE) received the B.E. (civil) and Bachelor of Surveying degrees (Honors) and the Ph.D. degree in water resources engineering from the University of Newcastle, Callaghan, NSW, Australia, in 1995 and 1999, respectively. His Ph.D. thesis was among the early pioneering research on the estimation of root-zone soil moisture from the assimilation of remotely sensed surface soil moisture observations.

He then joined the NASA Goddard Space Flight Center to implement his soil moisture work globally. In 2001, he moved to the Department of Civil and Environmental Engineering, The University of Melbourne, Melbourne, VIC, Australia, as a Lecturer, where he continued his soil moisture work, including the development of the only Australian airborne capability for simulating new satellite missions for soil moisture. In 2010, he was appointed as a Professor with the Department of Civil Engineering and Environmental Engineering, Monash University, Clayton, VIC, Australia, where he has continued this research. He is contributing to soil moisture satellite missions at NASA, ESA, and JAXA, as a Science Team Member for the Soil Moisture Active Passive (SMAP) mission and a Cal/val Team Member for the Soil Moisture and Ocean Salinity (SMOS) and Global Change Observation Mission—Water (GCOM-W), respectively.

Dr. Walker is an Australian Research Council Laureate Fellow.

**Synne Høyer Svendsen** received the Ph.D. degree from the University of Copenhagen, Copenhagen, Denmark, in 2004.

Her experience is within Arctic climate research with a particular focus on ice sheet modeling. She is currently working with GEUS, Geological Survey of Denmark and Greenland, as part of the GMMI (GEUS Mathematical Modeling of Icesheets) Group, Copenhagen.

**Stef Lhermitte** received the M.Sc. and Ph.D. degrees in bioscience engineering from KU Leuven, Leuven, Belgium, in 2002 and 2008, respectively.

He is a Remote Sensing Scientist with specific interest in the use of multi-source remote sensing and land surface modelling to assess cryosphere, atmosphere and ecosystem dynamics. Since 2022, he is a full-time Associate Research Professor at the Department of Earth and Environmental Science of KU Leuven, which he combines with a 20% position of Associate Professor the Department of Geoscience and Remote Sensing, TUDelft, Delft, The Netherlands. His research focuses on the development of innovative methods (e.g. machine learning) for assessing land-atmosphere interactions in order to assess the effect of climate (change) on the cryosphere, ecosystem dynamics, the hydrological cycle, sea level rise, etc. and their feedbacks on (future) climate.

**Yiwen Zhou** (Senior Member, IEEE) received the M.S. and Ph.D. degrees in electrical engineering from The George Washington University (GWU), Washington, DC, USA, in 2012 and 2017, respectively.

He was a Postdoctoral Scientist and a Lecturer with GWU, focusing on active remote sensing of vegetation and passive remote sensing of ocean salinity. He was a Research Scientist with Lincoln Agritech Ltd., Lincoln University, Christchurch, New Zealand, working on microwave sensor development. He is currently a Research Scientist with the Swiss Federal Institute for Forest, Snow and Landscape Research (WSL), Zürich, Switzerland, working on microwave remote sensing of the environment and accurate dielectric measurements of natural materials.

Dr. Zhou was a recipient of the URSI Young Scientist Award in 2021 and the IEEE Industrial Engineering Paper Award on Antenna Measurements and Applications in 2022. He is a Senior Member of URSI and a member of the ESA CryoRad Mission Advisory Group.